

Identified Isosteric Replacements of Ligands' Glycosyl Domain by Data Mining

Tinghao Zhang, Shenghao Jiang, Ting Li, Yan Liu, and Yuezhou Zhang*

Cite This: *ACS Omega* 2023, 8, 25165–25184

Read Online

ACCESS |



Metrics & More

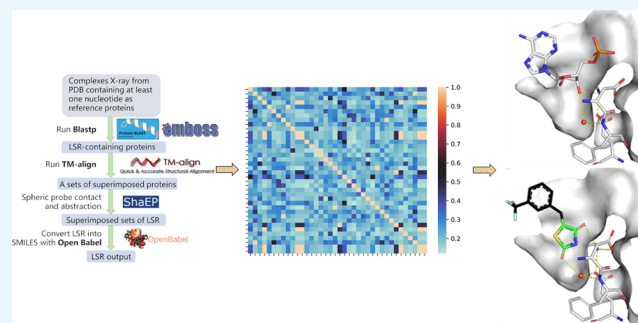


Article Recommendations



Supporting Information

ABSTRACT: Biologically equivalent replacements of key moieties in molecules rationalize scaffold hopping, patent busting, or R-group enumeration. Yet, this information may depend upon the expert-defined space, and might be subjective and biased toward the chemistries they get used to. Most importantly, these practices are often informatively incomplete since they are often compromised by a try-and-error cycle, and although they depict what kind of substructures are suitable for the replacement occurrence, they fail to explain the driving forces to support such interchanges. The protein data bank (PDB) encodes a receptor–ligand interaction pattern and could be an optional source to mine structural surrogates. However, manual decoding of PDB has become almost impossible and redundant to excavate the bioisosteric know-how. Therefore, a text parsing workflow has been developed to automatically extract the local structural replacement of a specific structure from PDB by finding spatial and steric interaction overlaps between the fragments in endogenous ligands and particular ligand fragments. Taking the glycosyl domain for instance, a total of 49 520 replacements that overlap on nucleotide ribose were identified and categorized based on their SMILE codes. A predominately ring system, such as aliphatic and aromatic rings, was observed; yet, amide and sulfonamide replacements also occur. We believe these findings may enlighten medicinal chemists on the structure design and optimization of ligands using the bioisosteric replacement strategy.



INTRODUCTION

Medicinal chemists are always keen to improve the potency of small molecules toward their biological targets using a variety of computational approaches, exemplified by high-throughput screening, quantitative structure–activity relationship, and fragment-based drug design. However, the success rate of the drug discovery project remains low,¹ while identification of potent compounds is expensive. From the pharmacodynamics perspective, a high potency of the ligand toward the receptor is positively correlated with high affinity. It is often observed that receptors recognize many endogenous ligands (EL) with an almost perfect binding mode. Hence, EL skeleton mimics using the partial structural replacement/exchange strategy are often under consideration to coin new drug candidates. Although a handful of means to obtain replacement building blocks are available, bioisosteric transformation is one among the prioritized strategies thanks to its conservative interactions with the receptor compared to the parent compound.²

Bioisosteric information could be attained either by applying medicinal chemistry knowledge or by mining databases. In the early stage, the obtainment of bioisosteres heavily depended on the experience of the practitioner, which possibly confined the application of bioisosterism. A novice chemist hardly knows the proper replacements of a specific fragment, and even the most experienced medicinal chemists may be unfamiliar with the ever-

increasing chemical knowledge. Undoubtedly, a group of possible bioisosteric alternatives (what or who) can be fished out from the massive published literature, but often fail to explain the mechanism (how or why) related to the replacements. The fundamental of isosteric transformability comes from the interaction conservatism among bioisosteres whose mechanism-of-action drug targets,³ mainly a variety of proteins, are the same or the sites of action remain identical. The molecular interaction information can be measured through experimental means such as isothermal titration calorimetry, while detailed insights can be observed through structural biology tools, exemplified by X-ray crystallography. The obtained information is often deposited into an open database and saved as computer readable files to facilitate the digitalized compilation of bioisosteric replacements. ChEMBL⁴ is a freely accessible database of more than 1.9 million small molecules with bioassay data curated from the literature. BIOSTER,⁵ for

Received: April 3, 2023

Accepted: June 9, 2023

Published: July 5, 2023



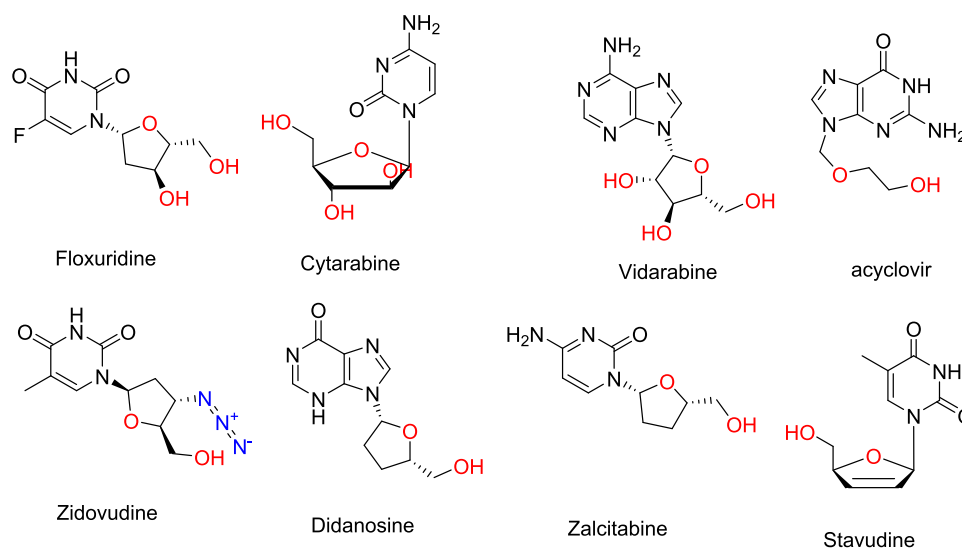


Figure 1. Drugs based on the modification of nucleoside ribose.

example, contains bioisosteric transformations collected from medicinal chemistry's literature published during the past four decades. Based on these data and the Matched Molecular Pair approach, molecules in ChEMBL that display bioisosteric features are identified, which also allows for the leverage of potential changes in biological properties with bioisosteric transformation; the above-mentioned information is currently presented as a SwissBioisostere database for both non-commercial and commercial users.⁶ Tuyishime et al.⁷ screen a database of more than 600 000 fragments to pinpoint bioisosteres that show similar steric and electronic features as the interest domain of molecules. Recently, bioisosteric analogues were identified by a deep neural network trained on a large corpus of experimentally validated analogues extracted from medicinal chemistry knowledge accumulated with nearly fifty years of efforts.⁸

Open accessible structural databases, including The Cambridge Structural Database (CSD)^{9,10} and PDB,¹¹ are rapidly growing, which provide another opportunity to obtain new bioisosteric replacements in a more automatic and robust manner. Through data mining and informatic curation,¹² massive bioisosteric information related to drug discovery and development can be disclosed. Frank et al.¹³ used crystal structure information from the CSD to inclusively study the geometrical and energetic aspects of the tetrazole-carboxylic acid bioisosterism by comparison of the conformational preferences and intermolecular interactions. After superimposition of holo proteins in the PDB with a reference protein, fragments residing in the same binding site are considered as potential bioisosteric candidates.¹⁴ Following a similar idea, the query and the reference ligands complexed with the same protein are fragmented into a set of fragments and compared with each other by their volume overlap; then, the pair with score higher than a given threshold is considered a bioisosteric pair.¹⁵ Further on, the similarity of binding site subpockets is quantified based on pharmacophore fingerprints, hence enabling both intra- and interfamily comparisons of proteins for bioisosteric replacements for ligand substructures.¹⁶ FragV-Lib,¹⁷ a virtual library of fragments, allows for bioisosteric replacements' identification based on a subgraph-matching tool that finds similar binding pockets according to their three-dimensional (3D) structures and chemical similarity of the

atoms. Desaphy et al developed sc-PDB-Frag,¹⁸ which implements bioisosteric searches by converting protein–ligand interaction patterns into graphs; bioisosteres are defined as any pair of ligands that share similar interaction patterns with their reference protein.

On the other hand, it is often difficult for those with noncomputational science background to obtain such information so as to refer to drug design and lead optimization. Therefore, the efforts toward developing user-friendly web servers that do not require computational or programming skills but are favorable to medicinal chemists to quickly search and get new ideas about possible bioisosteric replacements have been made. For instance, BoBER¹⁹ identified bioisosteric replacements using a local binding site; ProBiS ligands²⁰ sought for similar local spatial arrangements of physiochemically similar surface functional groups in the binding sites. Taking the liganded structure as an input and choosing specific substructures to replace, FragRep tries to find suitable bioisosteric fragments whose structures are different, while the interaction patterns with the protein pocket are similar.²¹

Ribose (a naturally occurring pentose sugar), commonly known as D-ribose, is an indispensable component of nucleotides and is primarily used for the assembly of RNA in all living organisms.²² It is also part of Riboflavin (vitamin B2),²³ adenosine triphosphate (ATP). The closely related sugar 2-deoxyribose is the building block of DNA.²⁴ ADP and AMP, the metabolites of ATP, are more stable and are commonly represented in the macromolecule complex as endogenous ligands. The ribose-containing molecules play critical pharmacology roles; for example, ADP ribose is a specific agonist of the purinergic P2Y1 receptor,²⁵ leading to Ca²⁺ mobilization in rat pulmonary arterial smooth muscle cell.²⁶ Cyclic ADP ribose and NAADP function as Ca²⁺ messengers and Ca²⁺ stores²⁷ in cells. Chemically, ribose is a five-member ring fragment composed of four carbon and one oxygen atoms. Three of the carbons are attached to hydroxyl groups (1', 2', and 3'). The fourth carbon attached to the fifth carbon atom is connected to a hydroxyl group (5'). Intuitively, the hydroxyl-rich structure makes ribose itself hydrophilic. In practice, the 1'- and 5'-hydroxyl of ribose are normally substituted or replaced by hydrophobic moieties.

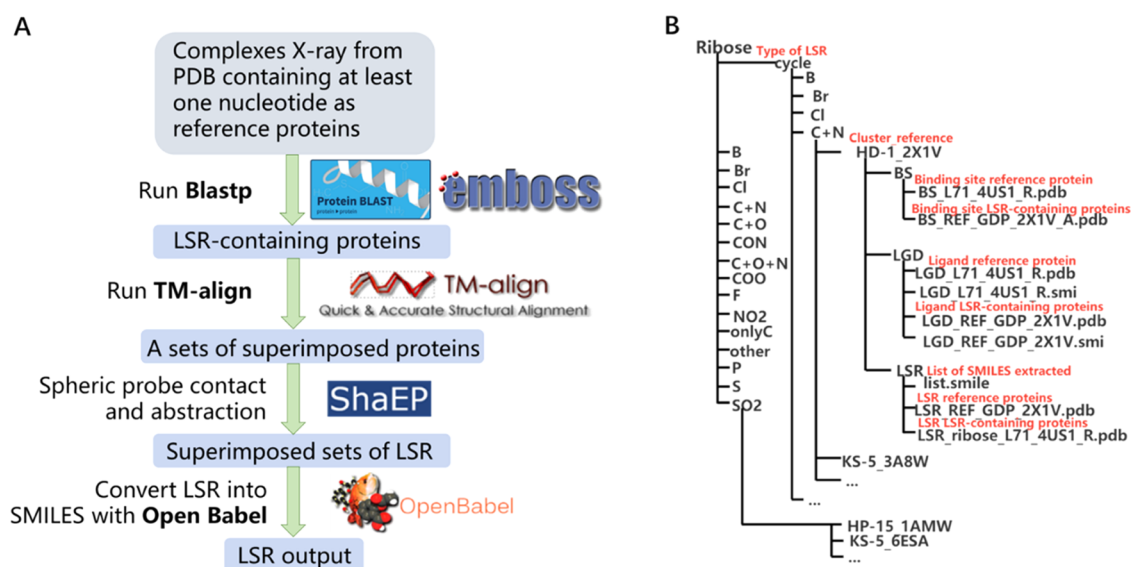


Figure 2. (A) Computational workflow. (B) Clustering graph of the data set.

Isosteric replacement of ribose groups is a classic practice in medicinal chemistry. For example, the modification of the ribose of nucleosides has led to the discovery of several drugs (Figure 1) such as the cancer therapeutic Floxuridine (FUdR, 5-fluoro-2-deoxyuridine),²⁸ where the 2'-hydroxyl of 5-fluoro-uridine is absent. Cytarabine (Ara-C) is a stereoisomer of cytidine with the D-ribose,²⁹ replaced with D-arabinose. Antivirals such as Vidarabine (Ara-A)³⁰ combine an adenine base and a D-arabinose sugar, and acyclovir hosts a truncated ribose structure compared to guanosine. Zidovudine, or azidothymidine,³¹ has the 3'-hydroxyl replaced by azido moiety. Other nucleoside analogues involved in inhibition of HIV-1 reverse transcriptase include Didanosine³² and Zalcitabine,³³ whose 2'- and 3'-hydroxyl of ribose are totally deleted. Blocking the puckering Zalcitabine deoxyribose ring by introducing a double bond between 2'- and 3'-carbon gave rise to another HIV-1 reverse transcriptase inhibitor, named Stavudine.³⁴ The systematic structure–activity relationship investigation of the nucleoside glycosyl domain also suggested the modification of ribose as a promising method toward successful drug development.³⁵ The above-mentioned attempts involve nucleosides in which the nitrogenous bases are attached to unnaturally occurring ribose via a β -N(1)-glycosidic bond and the ribose fragment undergoes stereoisomerism, hydroxyl truncation, or chemical modification, but nearly experiences the scaffold change. Hence, brand-new ribose isosteres/bioisosteres are highly desired to generate new analogues with improved properties.

Another endogenous ligand that underwent considerable modification of ribose³⁶ is cyclic ADP ribose (cADPR), a signalling molecule that has been shown to regulate Ca^{2+} mobilization in an intracellular manner. cADPR consists of two riboses, namely “northern” and “southern” ones.³⁷ The modification of cADPR ribose has led to a few chemical entities with useful pharmacology properties. For example, cyclic aristeromycin diphosphoribose (cArisDPR), featuring a furanose oxygen in “southern” ribose replaced by methylene, is a hydrolysis-resistant agonist with the half-life improved from 15 min of cADPR to 170 min of cArisDPR when incubated in sea urchin egg homogenates.³⁸ However, 3'-O-methyl-cADPR based on the “southern” ribose substitution became an antagonist of cADPR-induced Ca^{2+} release.³⁹ “Southern” ribose

appeared nonessential for the binding of cADPR to the human ADP-ribosyl cyclase CD38 catalytic domain since the replacement of the N9-ribose with a butyl chain generates an analogue that inhibits the hydrolysis of cADPR.⁴⁰ Similarly, the substitution of “northern” ribose by different alkene chains led to several cADPR analogues that were able to permeate in intact human Jurkat T-lymphocytes and act as agonists.⁴¹ 2'-NH₂-cADPR, with an amino group replacing the 2'-hydroxyl group of cADPR in the “northern” ribose, was an agonist in the T-lymphocyte system with the EC₅₀ of 7 μM as compared to 13 μM of cADPR⁴² and hydrolyzed nearly 100-fold slower than cADPR.⁴³ Other analogues of cADPR, such as cyclic ADP-4-thioribose, in which the “northern” ribose of cADPR was replaced by a 4-thioribose, were completely resistant in rat brain microsomal extract and induced the release of Ca^{2+} ions in a concentration-dependent manner with an EC₅₀ value of 36 nM in sea urchin egg homogenate testing, while cADPR and cADPcR gave the EC₅₀ value of 214 and 54 nM, respectively.⁴⁴

The substitution of the ribose often occurred in 2'- and 3'-position, where the numbers of both hydrogen bond donors and acceptors are reduced, which is also important for cell permeability, especially for ligands targeting the central nervous system. For example, the polarity of 4-nitrobenzylthioinosine reduced by replacing the ribose moiety with substituted (aryl)benzyl group. These chemically different replacements led to two equally active analogues with a K_i value of 39 nM.⁴⁵ In some cases, the ribose moiety is not important for the binding; therefore, replacement of the ribosyl group with a hydrophobic group might be rational because the polar hydroxyl groups of the ribose moiety are entropically unfavorable (require a higher desolvation energy) but have no contribution to the binding affinity. For instance, the substitution of the ribose moiety in compound 1.6 (IC₅₀, 100 μM) with the benzyl compound (IC₅₀, 91 μM) showed better potency.⁴⁶ If structure-based drug design or other computer tools suggest that the hydrogen bonds between the ribosyl hydroxyl and protein residues contributed little to the overall binding affinity,⁴⁷ while a hydrophobicity-dominated binding pocket preferred the hydrophobic moiety, then the replacement of ribose with an alkyl group should be settled. For example, cyclohexylethyl group replacement (IC₅₀, 97 μM) of ribose (IC₅₀, 118 μM) led to a comparable potency

Table 1. Number of Complexes and Ligands Collected in Each of the Datasets

	reference complexes in PDB	references complexes	collected replacement-containing proteins			number of structural isosteres in the data set, after the ShaEP filter
			total(isostere-containing + empty)	total(isostere-containing)	with binding sites identical to the reference protein	ribose
AMP	653	333	7042	4045	907	4045
ADP	2148	759	19 468	17 715	2381	17 698
ATP	1313	562	18 112	10 996	1832	10 980
USP	91	53	561	899	281	895
UDP	415	187	3476	1707	373	1703
UTP	70	36	1112	480	153	480
CSP	87	40	209	240	106	240
CDP	53	24	291	174	69	170
CTP	124	49	1288	807	159	807
SGP	121	56	390	384	163	384
GDP	1101	458	5729	9196	980	9188
GTP	765	176	3396	2934	338	2930

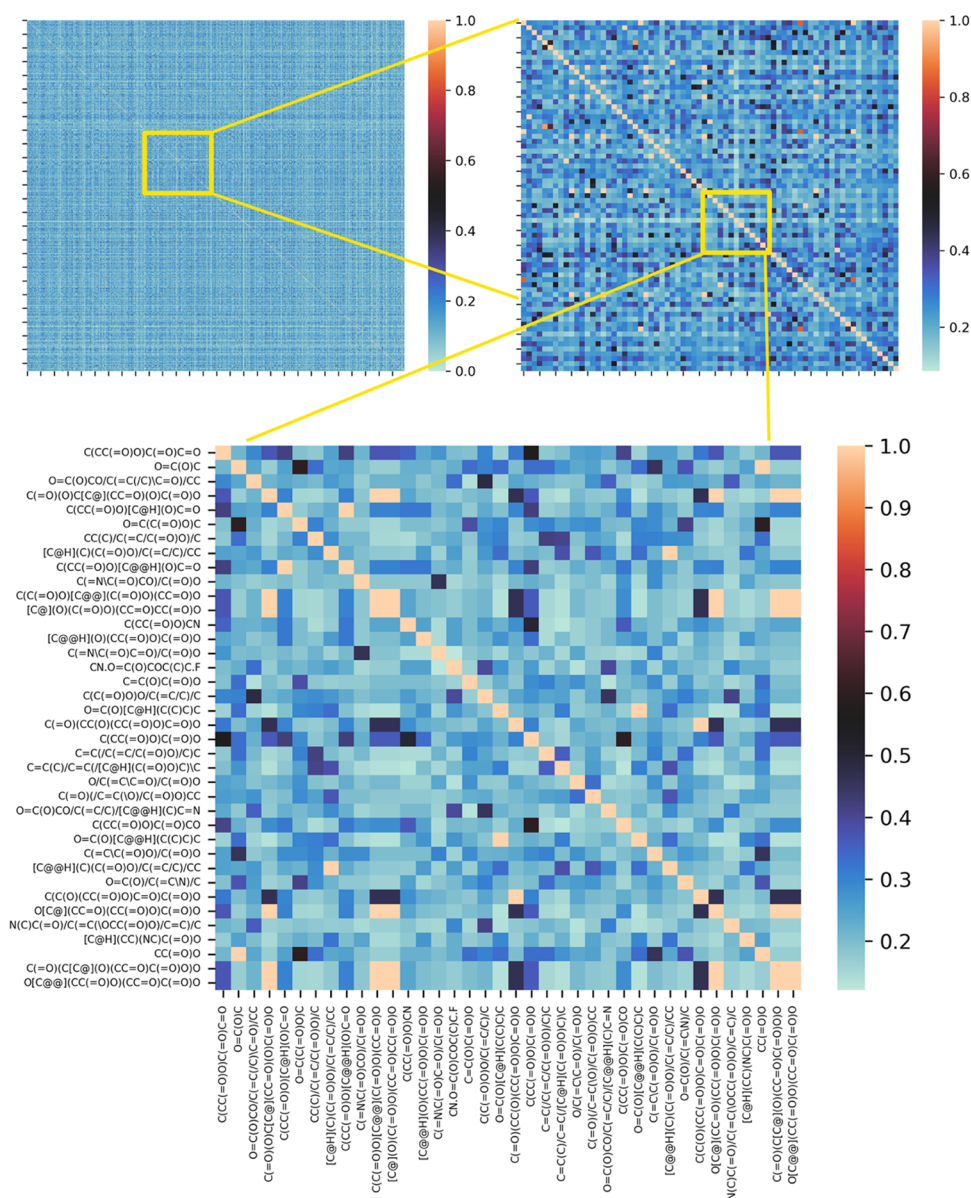


Figure 3. Tanimoto similarity between the extracted isosteres. Color coding according to Tanimoto similarity coefficients.

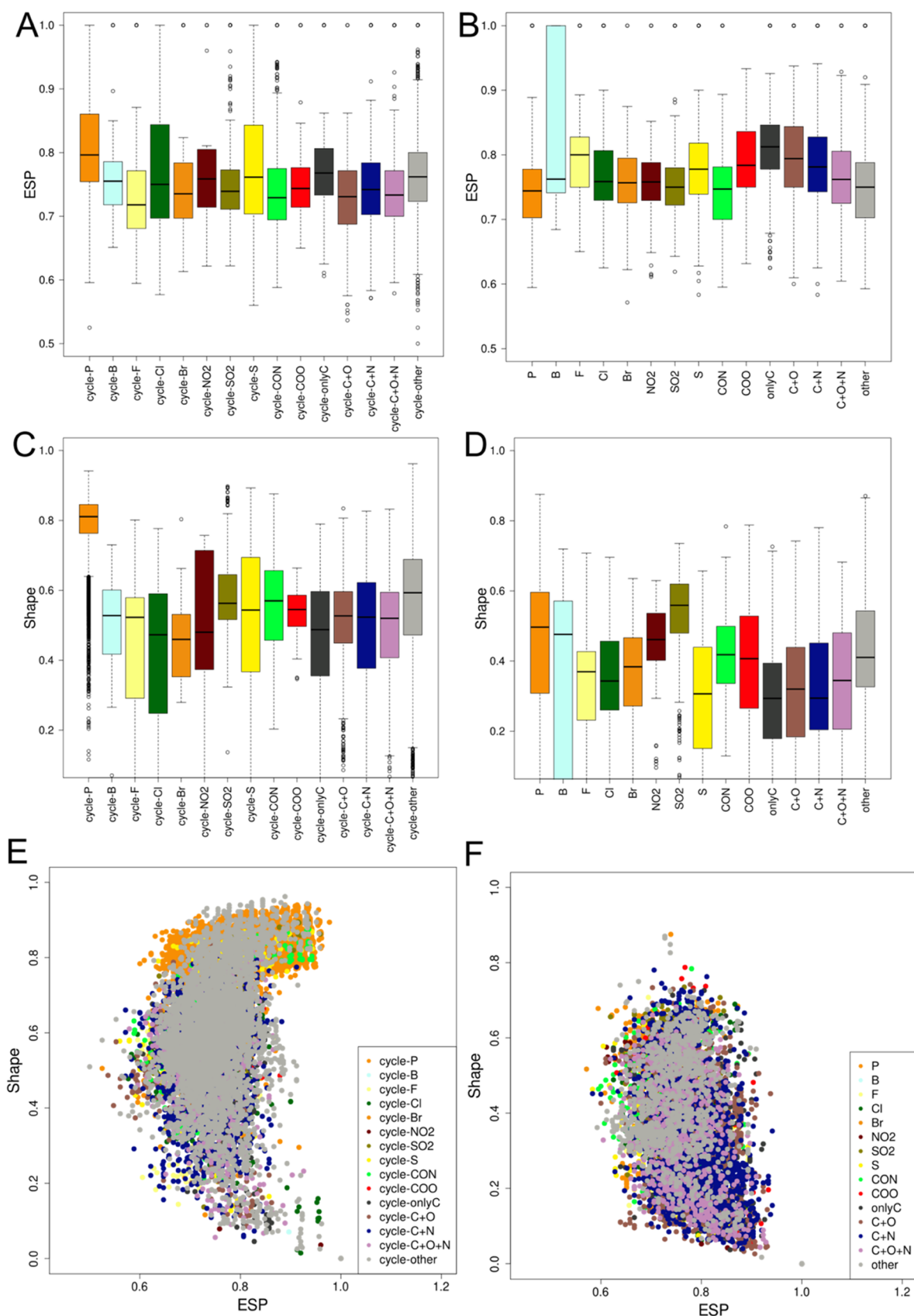


Figure 5. Segregation of the structural replacements according to their shape and electrostatic similarity scores compared to the reference ribose group calculated by ShaEP. (A, B) Boxplot of the electrostatic potential (ESP) overlap score for (A) cyclic and (B) noncyclic fragments. (C, D) Boxplots of the shape overlap score for (C) cyclic or noncyclic (D) fragments. (E, F) Scatterplots of these scores.

Table 2. Ribose Replacements that Are Structural Replacements of Ribose: Examples 1–5

no.	figure	target protein	target PDB code	target ligand	reference protein	reference ligand	replacements and comments
1	Figure 6A–C	<i>Bos Taurus</i> S6K1	4C36	ZO9	1Q24	ATP	cyclopropylmethyl, mutated LSR protein F54Y
2	Figure 6D–F	<i>H. sapiens</i> c-Src kinase	3EN5	KS4	3DQX	AMP	cyclobutyl
3	Figure 6G–I	<i>H. sapiens</i> phosphoinositide 3-kinase	3ML8	ML8	1E8X	ATP	cyclopentyl
4	Figure 6G–I	<i>H. sapiens</i> CDK2	1E1X	NW1	1B38	ATP	cyclohexyl
5	Figure 6M–O	<i>Influenza B virus</i> PB2	6EUX	BYB	SEFC	GTP	bicyclohexyl

Table 3. Specific Examples of SARs that Illustrate Ribose Replacements

Example 1 (Figure 6B) Compound s from reference ⁶¹	15e (Z09)	15a	15b	15c	15d	10	11
S6K1	0.0198	0.194	0.598	0.366	>100	0.34	6.98
IC ₅₀ (μM)		0.14 ⁶²					
PDB file	4C36	-	-	-	-	-	-

could automatically select the proper reference compounds for data extraction. In this study, we aim not only to identify the possible structural replacements of ribose moiety, but also understand the mechanism driving the occurrence of replacements, specifically from a molecular recognition perspective.

METHOD

We relied on five external programs to implement the workflow (Figure 2A): ① *Blastp* compares the query protein sequences to the sequence of PDB and outputs protein homologues with predefined statistical significance; ② *TM-align* generates an optimized residue-to-residue alignment of two protein structures and supplies their optimal superposition; ③ *ShaEP* calculates the fitness of the overlaid molecular fragments; ④ *Babel* translates the extracted molecular fragment into a SMILES string; and ⑤ *EMBOSS Needle* implements global pairwise sequence alignment. Having these tools compiled and integrated with Python scripts, the workflow firstly retrieves from PDB the three-dimensional structures of the protein that homologize with the protein bound with a nucleotide, designated as “reference ligands”. For the protein with multiple identical chains, only a single representative is kept and append PDB code_chain identifier is the output name. Secondly, the workflow acquires and aligns the homologues of each reference protein and preserves target proteins with a non-nucleotide ligand bound to an identical site of the reference ligand. Those with no ligand atom at the structural isostere site are removed. Thirdly, a probe sphere is created as such with its center being defined as the coordinate average of the atoms O2', O3', and O4' of the nucleotide, setting its radius at 2.5 Å. Atoms touchable by the probe sphere are extracted and considered as

the local structural replacements. Lastly, the fragments are categorized according to similar SMILES codes into 16 exclusive groups; the cycle group is complex and tedious, and is therefore further decomposed into 15 subgroups for clarity.

The empirically optimized filters used for the run are presented as follows: ① PDB structures with resolutions of 2.7 Å or better were kept; ② homologues were interrogated by a BlastP *e*-value of 10⁻¹⁰⁰; ③ manually built lists of prefiltered compounds AMP, ADP, ATP, ANP, ACP, AD9, NAD, AGS, APC, AOV, USP, UDP, UTP, SGP, GDP, GTP, CSP, CDP, and CTP in the pool of target ligands were excluded; ④ a binding site was defined as any amino acid with at least one atom within 4.5 Å of the bound reference ligand; a Shape component cut-off calculated by ShaEP higher than 0.2 was required. The similarity of extracted replacements was calculated based on Tanimoto similarity of SMILES codes.

RESULTS AND DISCUSSION

Data Curation. The prototype of data organization, SMILES-based folders, and contents of the running presented are almost identical to those already published by us,⁵³ but several features are mended: (1) the scripts, previously written in Python2.7, are rephrased according to the syntax of Python3.6 and made accessible through the GitHub collaborative code sharing platform at <https://github.com/Yuezhou-Project/IsoIdentifier>; (2) an updated version of the PDB database of May 2023 release (205133 structural deposition) is used and NMR entries are excluded; (3) nucleotide-binding proteins, i.e., proteins bound to not only AMP, ADP, ATP but also USP, UDP, UTP, CSP, CDP, CTP, SGP, GDP, and GTP are used as examples. The workflow (Figure 2A) provides the user with

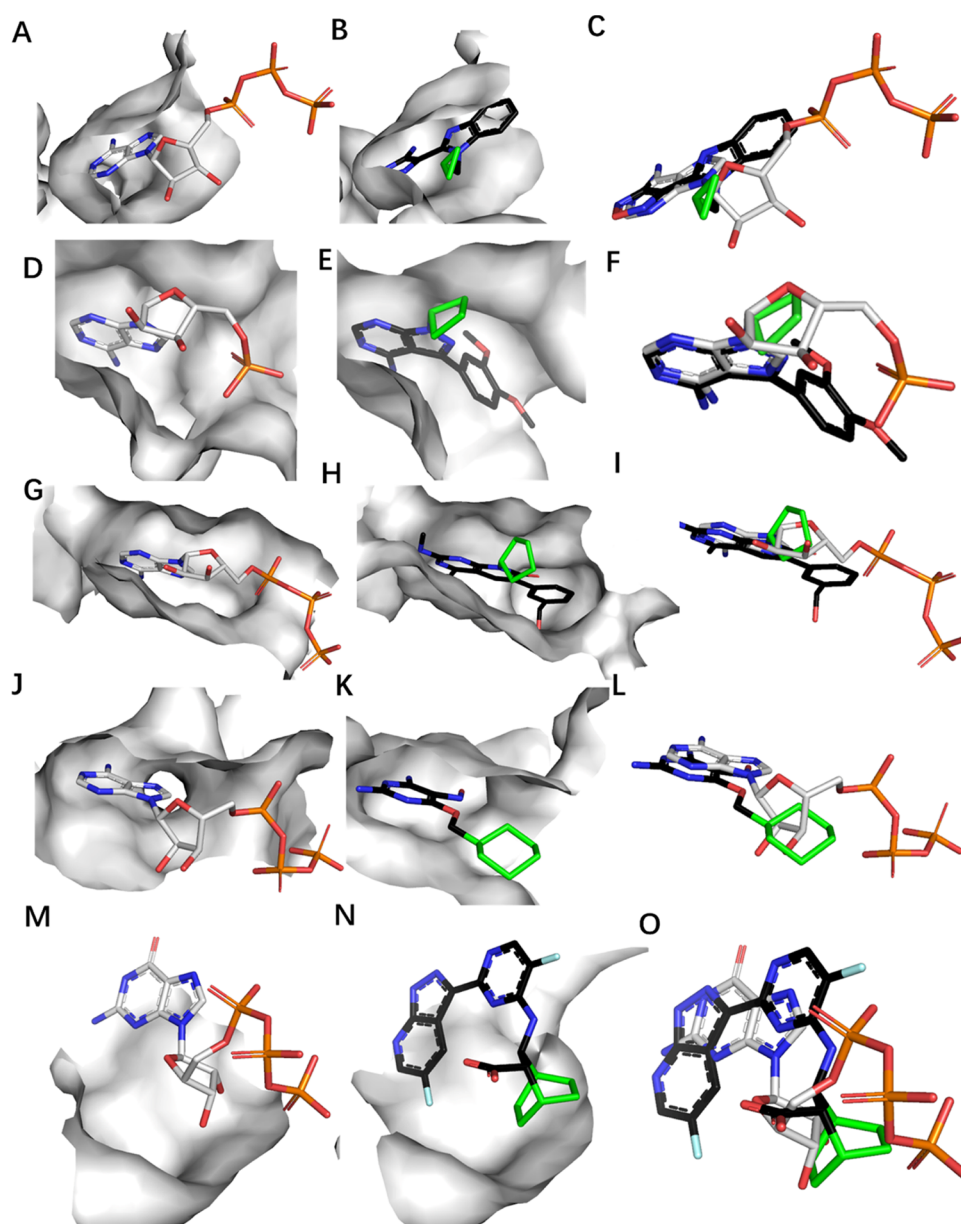


Figure 6. Selected examples of apolar aliphatic ring replacements of ribose. (A–C) *B. taurus* S6 kinase, ligand ZO9 (example 1, PDB codes 4C36 and 1Q24); (D–F) *H. sapiens* c-Src kinase, ligand KS4 (example 2, PDB codes 3EN5 and 3DQX); (G–I) *H. sapiens* phosphoinositide 3-kinase, ligand ML8 (example 3, PDB codes 3ML8 and 1E8X); (J–L) *H. sapiens* cyclin-dependent kinase 2, ligand NW1 (example 4, PDB codes 1E1X and 1B38). (M–O) *Influenza B virus* polymerase basic protein 2, ligand BYB (example 5, PDB codes 6EUX and 5EFC). (A, D, G, J, M) Reference proteins; (B, E, H, K, N) structural isostere (carbon atom is in green; the other part of carbon is in black) containing proteins; (C, F, I, L, O) close-up view of the ligand superimposition. In this and following figures, the ligands are named according to their PDB 3-letter codes, and the proteins are named according to PDB 4-letter codes. Putative hydrogen bonds and pi–pi staking interaction are shown as yellow dotted lines and the distance is labelled. The carbon atoms of ribose structural replacements in the target ligand are highlighted in green, while others are shown in black.

Table 4. Ribose Replacements That Are Bioisosteres of Ribose: Examples 6–7

no.	figure	target protein	target PDB code	target ligand	reference protein	reference ligand	replacements and comments
6	Figure 7A–C	<i>H. sapiens</i> PDE4B	3KKT	0CP	1TB5	AMP	tetrahydropyrimidin-2(1H)-one
7	Figure 7D–F	<i>H. sapiens</i> c-Src tyrosine kinase	2BDF	24A	3DQX	AMP	4-amino-cyclohexyl

analysis figures plotted in real time through interfacing with the R package. The workflow is applied to search the replacements of ribose moieties of these reference proteins (Table 1). In total, 2733 reference proteins and 49 520 local structural replacements are identified. The bias of these data concerning different nucleotides, for instance 759 cases of ADP binding protein versus only 24 cases of CDP, reflects the massive crystallo-

graphic and drug development project involving purine over pyrimidine derivatives (Table 1). The Tanimoto coefficients of the extracted isosteres (Figure 3) hardly tell what is the similarity threshold for ideal ribose structural replacements. In addition, the activity of a specific ligand toward the biological target is a combination of fragments; hence, a proper local replacement of

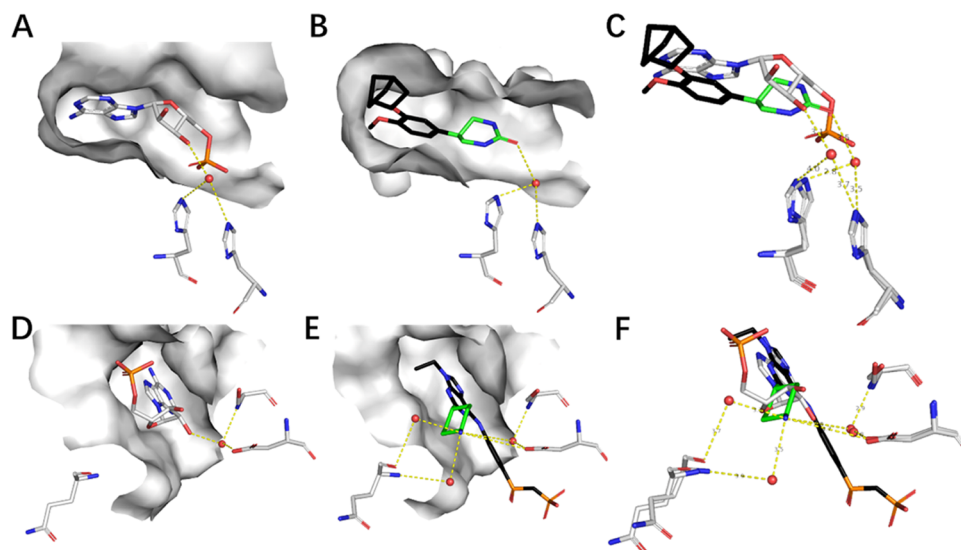


Figure 7. Selected examples of polar aliphatic ring replacements of ribose. (A–C) *H. sapiens* phosphodiesterase 4B (PDE4B), ligand OCP (example 6, PDB codes 3KKT and 1TB5). (D–F) *H. sapiens* c-Src kinase, ligand 24A (example 7, PDB codes 2BDF and 3DQX). (A, D) Reference proteins; (B, E) structural isostere (carbon atom is in green; the other part of carbon is in black) containing proteins; (C, F) close-up view of the superimposition.

Table 5. Ribose Replacements that Are Bioisosteres of Ribose: Examples 8–10

no.	figure	target protein	target PDB code	target ligand	reference protein	reference ligand	replacements and comments
8	Figure 8A–C	Influenza A virus endonuclease	6FS6	E4Z	SDEB	USP	benzene
9	Figure 8A,D,E	Influenza A virus endonuclease	5VPT	R07	SDEB	U5P	benzene
10	Figure 8F–H	<i>H. sapiens</i> hydrolase	3K3H	BYE	3DY8	SGP	chlorobenzene

the target moiety cannot guarantee a highly active molecule output.

The substructures extracted are hierarchically organized (Figure 2B) according to a decomposition SMILES code and the hierarchy is given as a text file (Supporting Information 1). The results are also archived into a folder and are downloadable, composed of structure files in pdb format and organized hierarchically into folders (Supporting Information 2). These data can be visualized by using computational tools such as PyMol.⁵⁸ Herein, 23 examples are discussed. The ligand–receptor recognition patterns of these examples are extrapolated in detail. In addition, their structure–activity relationship (SAR) is also appreciated if the data are available. For each of them, a diagram of ligand interaction is provided (Supporting Information 3) by LigPlot+.⁵⁹ Of these examples, 13 are of high resolution, better than 2.3 Å, among which 7 have been solved at a resolution better than 2.0 Å (resolution of the 18 examples as well as characteristics of the ligands, Supporting Information 4, Table 1).

To focus on the ribose replacements of most interest while putting aside many uninteresting or nearly identical ones, and ignore the very small replacements (Supporting Information 5) containing fewer than three atoms, a classification SMILES code-oriented paradigm is proposed for the extracted fragments with a structural fit on ribose groups. The same folder naming rules are followed as previously. The largest and complex folder is cycle 1; it is reasonable since ribose itself is a ring-based structure. This folder, therefore, is further divided into subfolders, and nominated as cycle.*; herein, * stands for the specific atom included in the extracted ring fragments. For instance, cycle.S denotes the extracted substructures in this folder containing the sulfur atom. Noticeably, the cycle.P folder is the most dominant (Figure 3) besides cycle.other folder, in

particular when uracil, cytosine, and guanine-binding proteins are references.

Enumeration of Ribose Structural Isosteres. Most of the ligands are found to be anchored at the adenine-ribose sites, as can be inferred from the higher number of replacements of adenylic ribose (Figure 4A–C) compared to guanylic, cytidylic (Figure 4G,H), and thymidinic ones (Figure 4J–L). Among all possible LSRs of ribose for different nucleotides except when referencing with ADP and ATP, cyclic moieties containing phosphorus (designated as cycle.P folder, the orange-colored pie in Figure 4A,D–L) remarkably outnumber other fragmental replacements. For instance, 7205 bioisosteric candidates were recognized in cycle.P category when GDP ribose was set as query, accounting for more than 94% identified ones in total. The phosphorus-containing cycle moiety sounds not so interesting to medicinal chemists, but biologists may pay attention to study the function of biomacromolecules.

Classification of the structural replacements is important for complicated tasks. Besides the SMILES codes-based data sorting method described above, we furthermore tried to cluster the fragments according to the shape and electrostatic potential scores calculated by ShaEP, which are integrated into the computational workflow. For each cluster of fragments, neither the electrostatic potential nor the shape favors the classification of the fragments, implying the difficulty in addressing this task (Figure 5). We therefore maintain the SMILES-based segregation, due to the advantage of helping the analysis and interpretation.

Apolar Aliphatic Ring. The data relative to the examples presented in this section and replacements of ribose are given in Table 2. The examples of the SARs discussed are presented in Table 3.

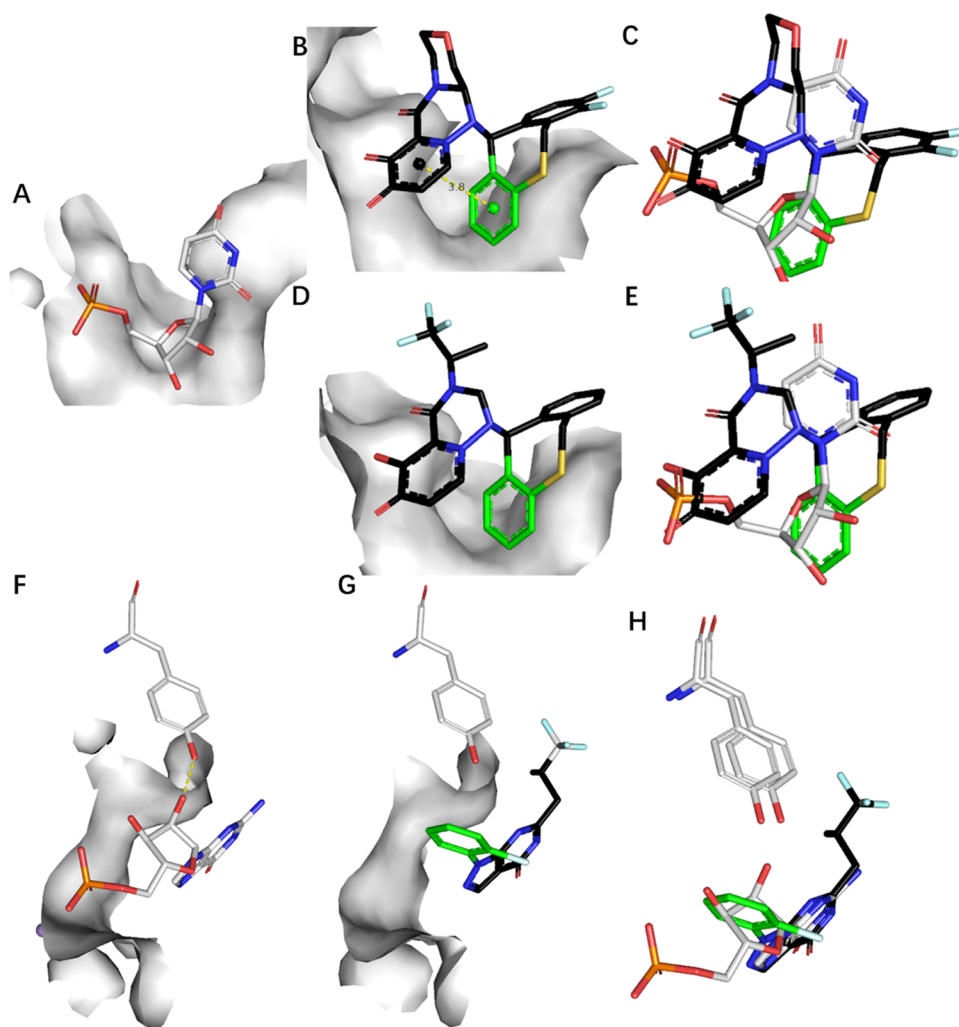


Figure 8. Selected examples of aromatic ring replacements of ribose. (A–C) Influenza A virus endonuclease, ligand E4Z (example 8, PDB codes 6FS6 and SDEB). (A, D, E) Influenza A virus endonuclease, ligand R07 (example 9, PDB codes SVPT and SDEB). (F–H) Homo sapiens hydrolase, ligand BYE (example 10, PDB codes 3K3H and 3DY8). (A, F) Reference proteins; (B, D, G) structural isostere (carbon atom is in green; the other part of carbon is in black) containing proteins; (C, E, H) close-up view of the superimposition.

Table 6. Ribose Replacements that Are Bioisosteres of Ribose: Examples 11–12

no.	figure	target protein	target PDB code	target ligand	reference protein	reference ligand	replacements and comments
11	Figure 9A–C	<i>H. sapiens</i> kinase Pim1	1YXX	LI7	1YXU	AMP	phenol
12	Figure 9A, E, F	<i>H. sapiens</i> kinase Pim1	4LMU	QUE	1YXU	AMP	catechol

The apolar aliphatic ring has commonly appeared in drug development projects,⁶⁰ but has hardly been addressed as an isostere of ribose. Our survey revealed several cases of its structural replacement as such. In bovine ribosomal S6 kinases RPS6KB1 (S6K1) (example 1, Figure 6A–C), ligand 15e in Table 3 offers the highest IC_{50} of 0.0198 μ M among *N*-1-substituted benzimidazole oxadiazole analogues.⁶¹ The compound with ethyl replacement (15c in Table 3, IC_{50} of 0.366 μ M) presents 18-fold lower IC_{50} toward S6K1, and the compound 15d with benzyl replacement completely loses activity, suggesting that a small and confined pocket exists; only the cyclopropylmethyl group can tightly fit the hydrophobic pocket formed by Gly50, Tyr54, Val57, and Phe327 (Figure 6B, Supporting Information 3 Figure S1). Besides, compounds containing this ring system had also been reported as inhibitors of the AGC kinases mitogen and stress-activated protein kinase (MSK1),⁶² Rho kinase, and ATP-binding site of protein

kinase.⁶³ Although the apolar aliphatic ring cannot mimic the hydrogen-bonding interactions of the ribose 2'- and 3'-hydroxyls toward the biological target, it is often observed that they occupy a space close to where the ribose ring of nucleoside binds, exemplified by KS4's⁶⁴ cyclobutyl moiety (Figure 6D–F, Supporting Information 3 Figure S3) in c-Src kinase, the cyclopentane group (Figure 6G–I, Supporting Information 3 Figure S5) of ML8⁶⁵ in phosphatidylinositol 3-kinase, and the cyclohexylmethyl group of NW1 in cyclin-dependent kinase (Figure 6J–L, Supporting Information 3 Figure S7).⁶⁶ A closer look underlines that the driving force anchoring the cycloaliphatic ring in proximity to the ribose is the hydrophobic interactions established by a hydrophobic patch on the glycine-rich loop of the receptor, assisted by the bulk of residues of valine for instance. The fused bicyclohexyl group of ligand BYB (VX-787N in ref 67) is packed with the Phe325 residue of influenza B cap-binding domain,⁶⁷ where the ribose moiety of GTP occupies

Table 7. Specific Examples of SARs that Illustrate Ribose Replacements

Example 12 (Figure 9 D) Compound from reference ⁷⁴	Quercetin (QUE)	Quercetagenin (MYU)	Myricetin (MYC)	Pentahydroxyflavone (MYF)
Pim1 IC ₅₀ (μM)	1.10	0.34	0.78	0.65
PDB file	4LMU ⁷⁴ /2O3P ⁷⁵	2O64 ⁷⁵	2O63 ⁷⁵	2O65 ⁷⁵

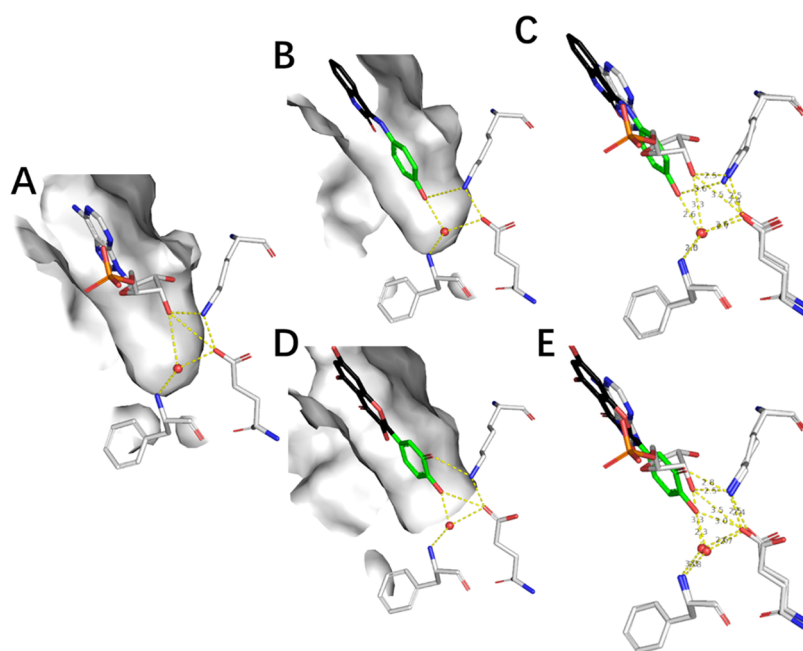


Figure 9. Selected examples of substituted aromatic ring replacements of ribose. (A–E) *H. sapiens* kinase Pim1, ligand LI7(B, C), QUE (D, E) (example 11 and 12, PDB codes 1YXX and 4LMU). (A) Reference proteins; (B, D) structural isostere (green) containing proteins; (C, E) close-up view of the superimposition.

Table 8. Ribose Replacements that Are Bioisosteres of Ribose: Examples 13–15

no.	figure	target protein	target PDB code	target ligand	reference protein	reference ligand	replacements and comments
13	Figure 10A–C	<i>H. sapiens</i> PDE4B	1XM6	SRM	1ROR	AMP	oxazolidin-2-one
14	Figure 10D–F	<i>H. sapiens</i> kinase Pim1	3VC4	0FS	1YXU	AMP	thiazolidinedione
15	Figure 10G–I	<i>H. sapiens</i> kinase Pim1	4K0Y	1OA	1YXU	AMP	pyrazolopyrimidone

the space of bicyclohexyl (Figure 6M–O, Supporting Information 3 Figure S9).

Polar Aliphatic Ring. The data relative to the examples presented in this section and replacements of ribose are specified in Table 4.

A six-membered heterocyclic ring can also be the structural replacement of ribose. In *H. sapiens*, PDE4B tetrahydropyrimidin-2(1*H*)-one is close to the ribose ring of AMP (Figure 7A) and the carbonyl of OCP (Figure 7B, Supporting Information 3 Figure S11) aligns with the 3'-hydroxyl of AMP ribose; a water is

conserved but shifted a bit between the structures of the complexes (Figure 7C) as a bridge between the two histidine residues and ligands' oxygen atoms, implying that 3'-hydroxyl of AMP is a hydrogen bond acceptor. The 4-amino-cyclohexyl substituent at the C2 position of the purine ring in 24A is oriented toward the ribose-binding portion of the AMP site (Figure 7D). Herein, the amino group (Figure 7E, Supporting Information 3 Figure S13) of 24A is the counterpart of 2'-hydroxyl in terms of the molecule recognition pattern as such a conserved water molecule is bifurcated and hydrogen-bonded

Table 9. Specific Examples of SARs that Illustrate Ribose Replacements

Example	(R)-Mesopram (5RM)	Filaminast (FIL)	Cilomilast (CIO)	Piclamilast (PIL)	(R)-Rolipram (ROL)
13 (Figure 10 B) Compound from reference ⁷⁸					
PDE4B IC ₅₀ (μM)	0.42	0.96	0.025	0.000041	0.57
PDB file	1XM6	1XLZ	1XLX	1XM4	1XMY

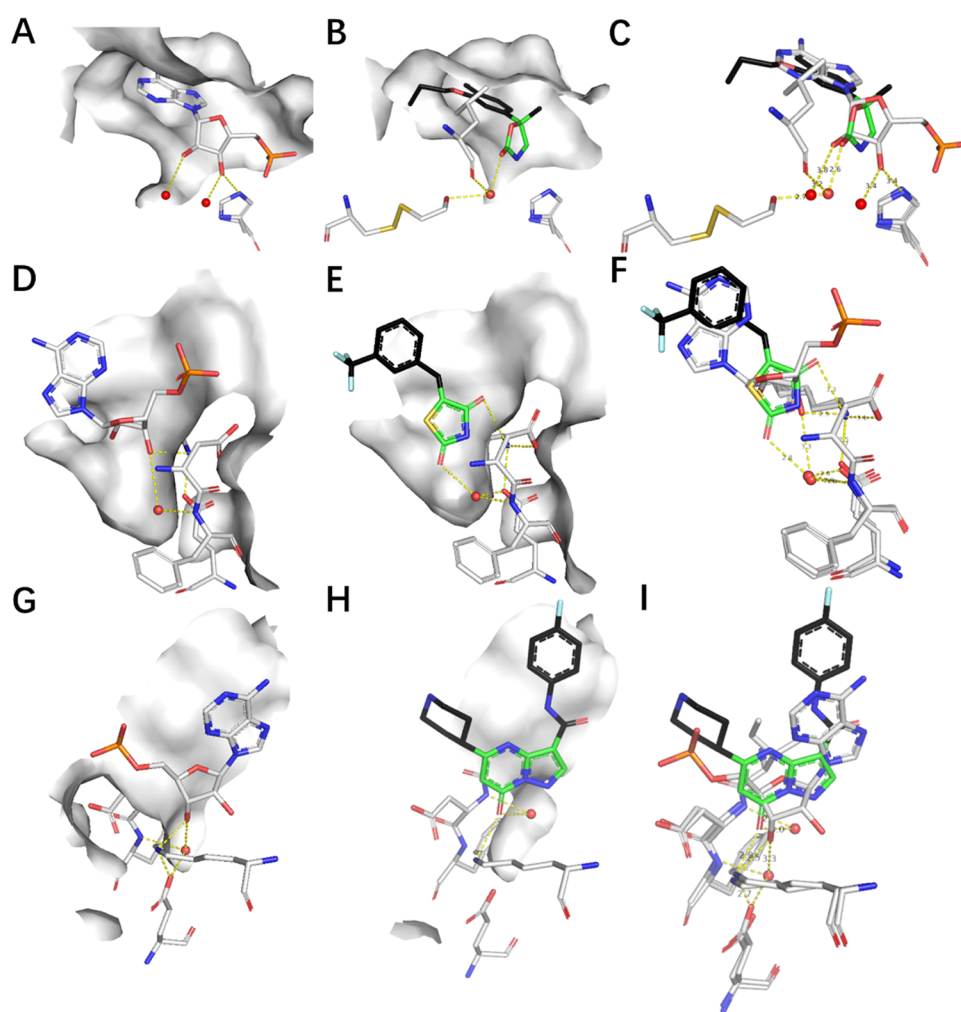


Figure 10. Selected examples of substituted heteroaromatic ring replacements of ribose. (A–C) *H. sapiens* PDE4B, ligand 5RM (example 13, PDB codes 1XM6 and 1ROR); (D–F) *H. sapiens* kinase Pim1, ligand 0FS (example 14, 3VC4 and 1YXU); (G–I) *H. sapiens* kinase Pim1, ligand 1OA (example 15, 4K0Y, and 1YXU). (A, D, G) Reference proteins; (B, E, H) structural isostere (green) containing proteins; (C, F, I) close-up view of the superimposition.

(Figure 7F) to the main NH of Ser345 and the side chain of Asp348.⁶⁸ Besides, the amino of 24A makes extensive contacts

with the backbone NH of Gln275 through a bridge water molecule.

Table 10. Ribose Replacements that Are Bioisosteres of Ribose: Examples 16–18

no.	figure	target protein	target PDB code	target ligand	reference protein	reference ligand	replacements and comments
16	Figure 11A–C	<i>H. sapiens</i> PDE4B	3L54	LXX	1E8X	ATP	pyridine
17	Figure 11D–F	<i>H. sapiens</i> kinase Pim1	4LL5	SK8	1YXU	AMP	imidazothiazole
18	Figure 11D, G–H	<i>H. sapiens</i> kinase Pim1	3BGQ	VX2	1YXU	AMP	triazolopyridazine

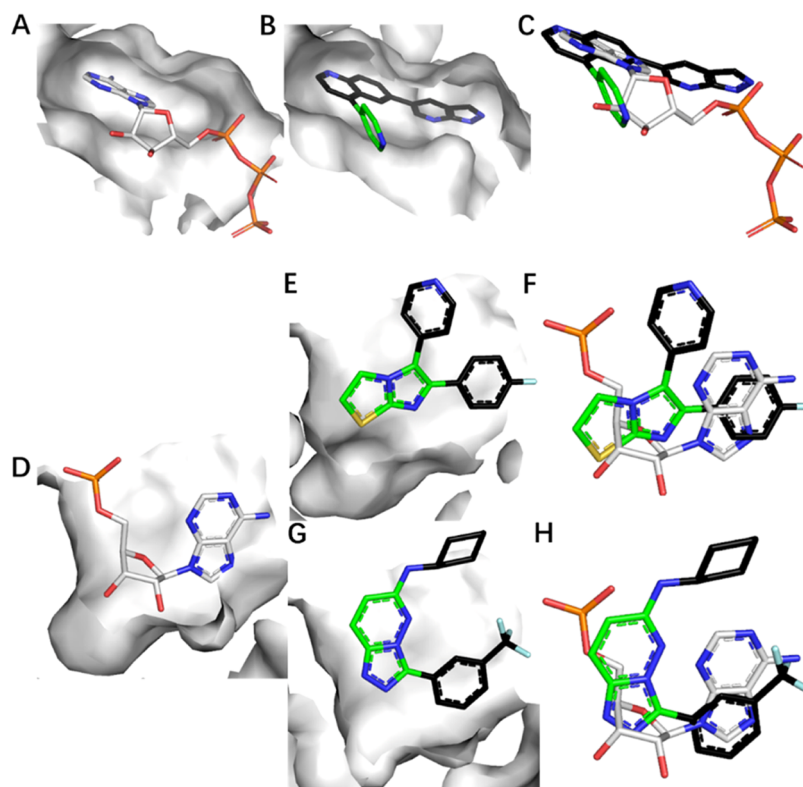


Figure 11. Selected examples of heteroaromatic ring replacements of ribose. (A–C) *H. sapiens* phosphoinositide 3-kinase α (PI3K α), ligand LXX (example 16, PDB codes 3L54 and 1E8X); (D–H) *H. sapiens* kinase Pim1, ligand SK8 (E, F), VX2 (G, H) (examples 17 and 18, PDB codes 4LL5, 3BGQ, and 1YXU). (A, D) Reference proteins; (B, E, G) structural isostere (green) containing proteins; (C, F, H) close-up view of the superimposition.

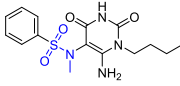
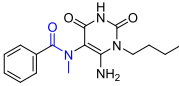
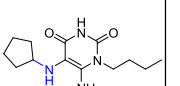
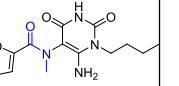
Table 11. Ribose Replacements that Are Bioisosteres of Ribose: Examples 19–22

no.	figure	target protein	target PDB code	target ligand	reference protein	reference ligand	replacements and comments
19	Figure 11A–C	<i>H. sapiens</i> Pim1 kinase	3VBV	0FK	1YXU	AMP	carboxamide
20	Figure 11D–F	<i>H. sapiens</i> death-associated protein kinase 3	3BHY	7CP	2W4J	ADP	γ -lactam
21	Figure 11G–I	<i>H. sapiens</i> cyclic GMP-AMP synthase	6MJW	JUJ	4JLZ	UTP	cycle-amide
22	Figure 11J–L	<i>P. aeruginosa</i> PAO1	4B42	942	4HO9	UTP	benzamide

Aromatic Ring. The data relative to the examples presented in this section and replacements of ribose are given in Table 5. The UMP binding pocket of influenza A virus endonuclease is open and large (Figure 8A); therefore, it can accept molecules with different scaffolds. For instance, the T-shaped ligand (PDB code: ON8) can access the pocket, while it has no fragment overlaid with the USP ribose.⁶⁹ The butterfly-like ligand E4Z co-crystallizes with influenza A virus endonuclease, with one wing consisting of a metal chelating polar head group and another wing, a lipophilic tail group that makes van der Waals contacts with specific residues of the active site pocket (Figure 8B, Supporting Information 3 Figure S15). One of the tail-group aromatic rings of E4Z spaces the position of USP ribose (Figure 8C), intramolecularly π - π stacked with dihydropyridine (centroid distance of benzene...pyridine 3.8 Å); the binding of

E4Z to influenza A virus endonuclease significantly stabilizes the structure, with more than +32 °C ΔT_m from 46 to 78 °C,⁷⁰ similar to E4Z, by replacement of morpholine with trifluoropropane to obtain the analogue compound (Figure 8D, Supporting Information 3 Figure S17) R07,⁷¹ which has an identical binding mode (Figure 8E) to the aromatic ring occupying the position of ribose. The chloro-benzyl group of ligand BYE contacts via hydrophobic interaction (Figure 8G, Supporting Information 33 Figure S19) with PDE9's subpocket, which is made of residues His252, Met365, Leu420, Tyr424, and Phe456;⁷² the subpocket is also occupied by the ribose (Figure 8F, H) of 5GP, which is an endogenous ligand of PDEs.⁷³ Ligand BYE had an IC₅₀ of 88 nM for the wild-type PDE9A, and its enantiomer PDB is 4 times more potent (22 nM), attributed

Table 12. Specific Examples of SARs that Illustrate Ribose Replacements

Example	22	1 (HNR)	3 (942)	4 (NIQ)	5
(Figure 12 K)					
Compound from reference ⁸³					
IC ₅₀ (μM)		0.21 ± 0.03	n.d.	n.d.	5.9 ± 2.9
% inhibition at 10 μM		100	30.3 ± 4.1	30.0 ± 2.0	71.1 ± 1.2
% inhibition at 60 μM		100	75.7 ± 3.9	39.4 ± 4.6	100
PDB file		4ARW	4B42	4B2X	-

to different orientations of the fluoromethyl groups of BYE and PDB.

Substituted Aromatic Ring. The data relative to the examples presented in this section and replacements of ribose are given in Table 6. Examples of the SARs discussed are presented in Table 7.

In the Pim1-AMP co-crystal structure, the ribose group goes deep into the pocket and the 3'-OH joins an extensive hydrogen bond network formed inside the pocket by Lys67, Glu89, the backbone NH of Phe187, and a water molecule (Figure 9A). The phenol of LI7⁷⁴ sits inside the same pocket (Figure 9B, Supporting Information 3 Figure S21), with its hydroxyl group participating in the highly conserved water-mediated hydrogen bond network near Lys67, Glu89, and Phe187 in a direction similar to the 3'-OH of AMP (Figure 9C). The same pocket also accommodates the QUE catechol fragment (Figure 9D, Supporting Information 3 Figure S23), with its two hydroxyl groups and the water molecule being involved (Figure 9E) in the hydrogen bond network.⁷⁵ Ligand QUE in Table 7 exhibits an IC₅₀ activity of 1.10 μM (Table 7 in ref 75) toward Pim1; the OH group addition at position 6 of the QUE A ring gives MYU with an IC₅₀ of 0.34 μM, the highest inhibitory among flavonoids analogues; the additional OH group at 5' position of the B ring results in MYC with an IC₅₀ of 0.78 μM, a slight activity increase; the addition of OH group at the 5' position of the B ring and the deletion of the OH group at position 3 of the C ring yields an MYF IC₅₀ of 0.65 μM, nearly double the activity of QUE. Of these four compounds co-crystallized with Pim1, QUE and MYU orient the B ring (see reference⁷⁶) inside the binding pocket, whereas MYC and MYF flip the B ring out toward the solvent.

Substituted Heteroaromatic Rings. The data relative to the examples presented in this section and replacements of ribose are given in Table 8. The examples of the SARs discussed are presented in Table 9.

Among *H. sapiens* phosphodiesterase 4B (PDE4B) dialkoxyphephenyl inhibitors, the oxazolidinone moiety of mesopram (SRM)⁷⁷ inserts into the AMP ribose (Figure 10A) and protrudes into the M pocket, with its carbonyl participating in the hydrogen bond network involving the backbone carboxyl oxygen of Leu510, Cme430, and a conserved water molecule (Figure 10B, Supporting Information 3 Figure S25), playing an identical role to the 2'-OH of AMP (Figure 10C). (*R*)-Mesopram provides an IC₅₀ of 0.42 μM toward PDE4B; its analogue rolipram (ROL) with a smaller pyrrolidinone substituent results in a lower binding affinity of IC₅₀ 0.57 μM, the hydroxamate substituents of filaminast (FIL) form similar interactions with the residue in the M pocket and hence has a similar binding affinity of 0.96 μM; the carboxycyclohexyl substituent of CIO forms several more interactions with the residues in the M pocket compared to the substituents in FIL and SRM and therefore is a more potent inhibitor with an IC₅₀ of 0.025 μM, about 17-fold increase of binding affinity; impressively, the extensive interactions formed between piclamilast (PIL) and the active site residue make it the most potent molecule in this series of inhibitors with an IC₅₀ of 4.1 × 10⁻² nM toward PDE4B. In *H. sapiens* kinase Pim1, the thiazolidinedione group of 0FS (Figure 10E, Supporting Information 3 Figure S27) is perpendicular (Figure 10F) to the ribose of AMP (Figure 10D), with one of its carbonyls hydrogen bonding to Lys67, another carbonyl participating in the hydrogen bond network containing the backbone NH of Phe 160, Glu 162 residue, and a conservative water molecule, similar

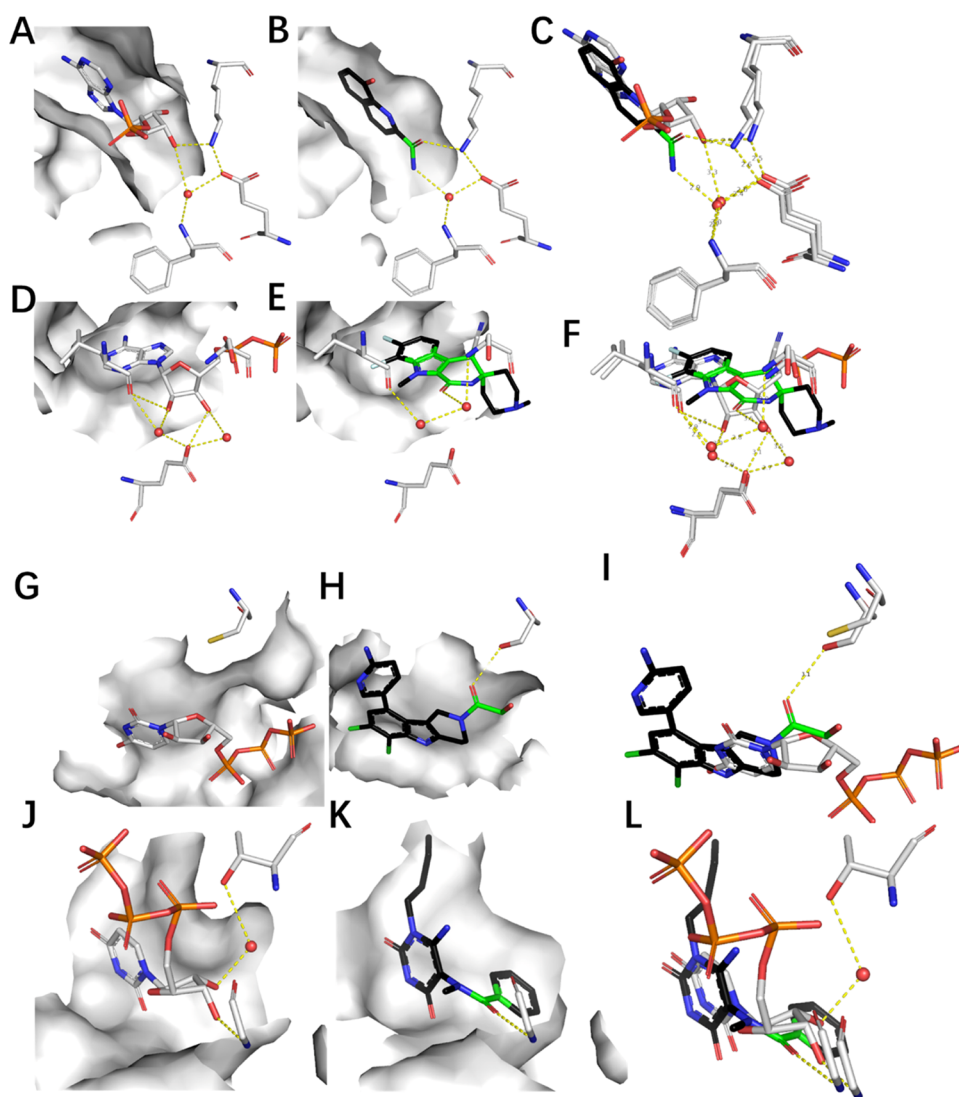


Figure 12. Selected examples of amide replacements of ribose. (A–C) *H. sapiens* Pim1 kinase, ligand 0FK, (example 19 PDB codes 3VBV and 1YXU); (D–F) *H. sapiens* Death-associated protein kinase 3, ligand 7CP (example 20, PDB codes 3BHY and 2W4J). (A, D) Reference proteins; (B, E) structural isostere (green) containing proteins; (C, F) close-up view of the superimposition. (G–I) Homo sapiens cyclic GMP-AMP synthase, ligand JUJ (example 21 PDB codes 6MJW and 4JLZ); (J–L) *Pseudomonas aeruginosa* glucose-1-phosphate thymidyltransferase (RmlA), ligand 942 (example 22 PDB codes 4B42 and 4HO9).

Table 13. Ribose Replacements that Are Bioisosteres of Ribose: Examples 23–24

no.	figure	target protein	target PDB code	target ligand	reference protein	reference ligand	replacements and comments
23	Figure 13A–C	<i>H. sapiens</i> CDK2	2VTH	LZ2	4I3Z	ADP	sulfonamide (terminal)
24	Figure 13D–F	<i>H. sapiens</i> kinase Pim1	1YDS	IQS	2W4J	ADP	sulfonamide (linker)

to the role of AMP 3'-OH (Figure 10E). Noticeably, the continuous fragment-based optimization of OFS has led to the most potent compound (6 in ref 78) with an IC_{50} of 0.42 nM toward Pim1. In Pim1, the pyrazolopyrimidone core (Figure 10H, Supporting Information 3 Figure S29) of 10A lies on the space of AMP ribose (Figure 10G), with the hydroxyl group directly hydrogen bonding (Figure 10I) to the Lys67 residue amine, and pyrazolopyrimidine interacting with the Val52 residue through hydrophobic interaction.⁷⁹

Heteroaromatic Rings. The data relative to the examples presented in this section and replacements of ribose are given in Table 10.

In PI3K α , the pyridine moiety of LXX (Figure 11B, Supporting Information 3 Figure S31) interlocks with the

ribose of ATP (Figure 11A), with 2'-hydroxyl (Figure 11C) passing across the heteroaromatic ring⁸⁰ and achieving an IC_{50} of 7 nM. Structurally, ribose is regarded as the transition between purine/pyrimidine and phosphate; its structural replacement may also take the same role. Kinase inhibitor SK8 (SKF86002 in reference⁷⁵) binds to the AMP binding sites (Figure 11D) of kinase Pim1, and makes many hydrophobic interactions with imidazothiazole shouldering both pyridine and the fluoro-substituted phenyl ring (Figure 11E, Supporting Information 3 Figure S33). SK8 does not form direct hydrogen-bonding interactions with protein (Figure 11F), hence has no kinase inhibition detected even at 100 mM. However, the triazolopyridazine replacement (Figure 11G, Supporting Information 3 Figure S35) of VX2 accepts a hydrogen bond from

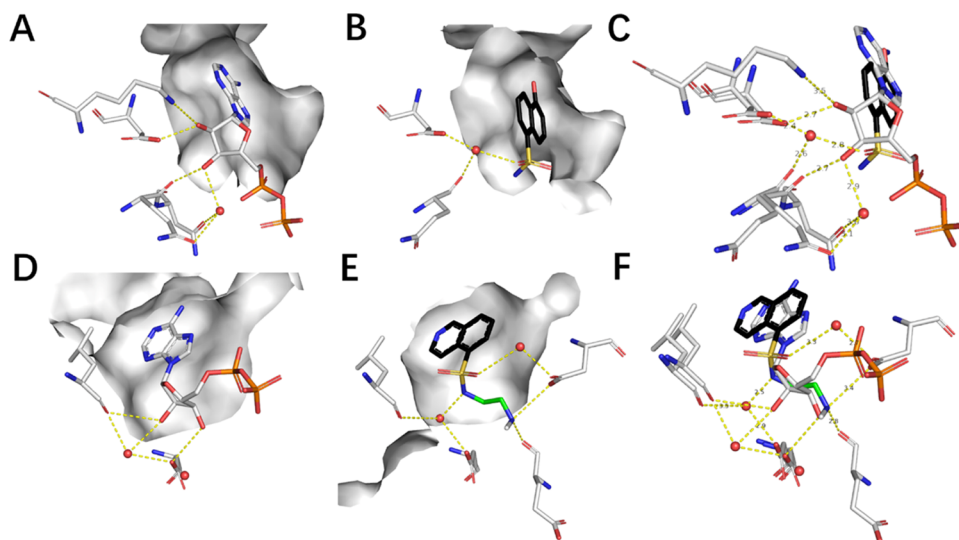


Figure 13. Selected examples of sulfonamide replacements of ribose. (A–C) *H. sapiens* cyclin-dependent kinase 2 (CDK2), ligand LZ2 (example 23 PDB codes 2VTH and 4I3Z); (D–F) *B. taurus* CDK2, ligand IQS (example 24, PDB codes 1YDS and 2W4J). (A, D) Reference proteins; (B, E) structural isostere (green) containing proteins; (C, F) close-up view of the superimposition.

the side chain of Lys67, giving a dramatically increased inhibition constant K_i of 0.011 μM ,⁸¹ interlocked with the ribose of AMP (Figure 11H).

Amide. The data relative to the examples presented in this section and replacements of ribose are given in Table 11. The examples of SARs discussed are presented in Table 12.

The carboxyl oxygen of OFK (Figure 12B, Supporting Information 3 Figure S37) directly accepts a hydrogen bond from the Lys67 residue, while the NH of OFK, backbone NH of Phe 160, and residue of Glu62 form a hydrogen bond network⁷⁸ in the AMP binding site of Pim1 (Figure 12C); together, the terminal amide of OFK is bifurcated and replaced by the 3'-OH of AMP (Figure 12A). In the DAPK3 complex, 7CP's γ -lactam carbonyl establishes a hydrogen bond with a water molecule (Figure 12E, Supporting Information 3 Figure S39) in the active site,⁸² in which AMP ribose (Figure 12D) and the pyridone ring interweave (Figure 12F). Ligand JUJ (G150 in reference⁸³) is situated by the GTP binding pocket of cyclic GMP-AMP synthase (Figure 12G), with the part of the hydroxyl-ethanone side chain attached to the nonplanar six-membered ring (Figure 12I) and hydrogen-bonded with the Ser434 residue hydroxyl (Figure 12H, Supporting Information 3 Figure S41). *P. aeruginosa* RmlA was screened against a compound library and HNR was identified (compound 1 in Table 12) as an inhibitor, showing 100% inhibition at 10 μM ; both 942 and NIQ (compounds 3, 4 in Table 12 correspondingly) show about 30% inhibition at 10 μM , while 942 is 36% more potent than NIQ at 60 μM concentration.⁸⁴ Ligand 942 is a commercially available analogue of HNR while less potent, indicating that replacement of the sulfonamide in HNR by an amide in 942 or an alkyl substituent in NIQ was unfavorable. Herein, the carboxyl oxygen of the amide in 942 hydrogen bonds to the backbone (Figure 12K, Supporting Information 3 Figure S43) NH of Gly115, which forms an equivalent interaction with the 3'-OH of UTP (Figure 12J,L).

Sulfonamide. The data relative to the examples presented in this section and replacements of ribose are given in Table 13.

The sulfonamide moiety of LZ2 forms a water-mediated hydrogen bond with the backbone carbonyl of Gln131 and with the carboxylate side chain of Asp86 (Figure 13B, Supporting

Information 3 Figure S45), partly occupying the ribose (Figure 13A) pocket,⁸⁵ and gives an IC_{50} of 120 μM toward CDK2. Isoquinolinesulfonamide protein kinase inhibitor IQS is an ATP-competitive inhibitor toward cAPK, giving an IC_{50} of 1.2 μM . When superposed with ATP (Figure 13D), it shows that one of the SO_2 oxygens (O-2) of the IQS roughly overlaps (Figure 13E, Supporting Information 3 Figure S47) with the O-4' oxygen of the ribose ring (Figure 13F); O-1 is close to the amide of Gly50, orienting for a weak interaction; a water molecule bridges one IQS sulfonyl oxygen to the carboxylate residue of Asp184. Another water molecule makes bidentate contacts with the Glu127 residue carboxylate and backbone carbonyl of Leu49.⁸⁶

Comparison with Other Tools and Approaches. Many (bio)isosteric replacement tools are available to facilitate lead compound optimization in drug discovery. For instance, MB-Isoster⁸⁷ identifies substituents to replace a selected subregion by querying an internal library containing bioisosteric candidates obtained from the SAR studies reported in medicinal chemistry journals. It is possible that SAR enumeration qualitatively depicted favorable or unfavorable potential when appending or removing functional groups at specific substitution points, but failed to explain why some substitutes result in activity gain, while others have no contribution and even lead to the activity loss. This is due to the lack of structural information on the ligand–receptor complex; therefore, recent bioisosteric screening applications have tried to incorporate this information, exemplified by calculating pharmacophore fingerprint of the binding site subpocket similarity to search bioisosteric candidates. This ligands' feature-focused approach, however, is hardly differentiated from pharmacophore search. Our approach on the other hand paid attention to both the ligand and the receptor; besides, our screening is confined to homologous proteins, assumed to yield an more suitable bioisosteric replacement candidates. Obviously, our treatment possibly misses out potential bioisosteres between heterogeneous proteins. Some commercial tools performed well, such as BIOSTER and SwissBioisostere, but their applications might be confined due to economic concerns. Our workflow is developed based on the openly accessible database PDB and by using the

very popular programming languages Python and R. More generally, the current workflow has been integrated into the Django framework, aiming to develop a free web server to facilitate practitioners without computer background designing drugs using the bioisosteric strategy.

CONCLUSIONS

The robustness of our previously developed workflow is demonstrated by designating glycosyl ribose fragments of ligands as the query moiety. By superimposing X-ray structures of homologous proteins, we extracted 49 520 structural isosteres, which partially reflected the chemical features of ribose and therefore can be considered as a rational structural replacement. Among them, we discussed 23 typical examples, categorized as apolar/polar aliphatic rings, substituted aromatic/heteroaromatic rings, amides, and sulfoamide surrogates. In particular, the SAR analysis of a few cases is enumerated, with the correlation of these replacements/deviations with the biological activities since structural optimization remains the fundamental mission of medicinal chemistry. During the isosteres' identification process using this protocol, it was realized that the water in the ligand binding site is an important mediator to drive isostere interchange, but was poorly understood, which might be worthy of investigation in future. Of course, it would be more eye-catching to generalize the workflow into a user-friendly open-source browser application for any chemical fragments of interest.

ASSOCIATED CONTENT

Data Availability Statement

Scripts enabling reproduction of all of the results obtained in the study are available at <https://github.com/Yuezhou-Project/IsoIdentifier>.

Supporting Information

The Supporting Information is available free of charge at <https://pubs.acs.org/doi/10.1021/acsomega.3c02243>.

Text file containing the hierarchically organized SMILES code (ZIP)

Hierarchically organized local structural replacements of ribose (ZIP)

Examples of local structural replacement of ribose (Table 1) (PDF)

ribose_small (ZIP)

Exemplified ligand–receptor interaction depicted by LigPlot+ (PDF)

Ignored replacements who are very small fragments (PDF)

AUTHOR INFORMATION

Corresponding Author

Yuezhou Zhang – Xi'an Institute of Flexible Electronics (IFE) and Xi'an Institute of Biomedical Materials & Engineering (IBME), Northwestern Polytechnical University, Xi'an 710072, China; Ningbo Institute of Northwestern Polytechnical University, Frontiers Science Center for Flexible Electronics (FSCFE), Key laboratory of Flexible Electronics of Zhejiang Province, Ningbo Institute of Northwestern Polytechnical University, Ningbo 315103, China; orcid.org/0000-0002-8560-5716; Email: iamyzzhang@nwpu.edu.cn

Authors

Tinghao Zhang – Xi'an Institute of Flexible Electronics (IFE) and Xi'an Institute of Biomedical Materials & Engineering (IBME), Northwestern Polytechnical University, Xi'an 710072, China

Shenghao Jiang – School of Computer Science, Northwestern Polytechnical University, Xi'an 710072, China

Ting Li – Xi'an Institute of Flexible Electronics (IFE) and Xi'an Institute of Biomedical Materials & Engineering (IBME), Northwestern Polytechnical University, Xi'an 710072, China

Yan Liu – Xi'an Institute of Flexible Electronics (IFE) and Xi'an Institute of Biomedical Materials & Engineering (IBME), Northwestern Polytechnical University, Xi'an 710072, China

Complete contact information is available at:

<https://pubs.acs.org/10.1021/acsomega.3c02243>

Notes

The authors declare no competing financial interest.

ACKNOWLEDGMENTS

This research was sponsored by the Joint Research Funds of the Department of Science & Technology of Shaanxi Province, Northwestern Polytechnical University (No. 2020GXLH-Z-017), funded by Ningbo Natural Science Foundation (No. 202003N4006).

LIST OF ABBREVIATION

PDB:Protein data bank; LSR:local structural replacement; EL:endogenous ligands; CSD:Cambridge Structural Database; ATP:adenosine triphosphate; cADPR:cyclic ADP ribose; cArisDPR:cyclic aristeromycin diphosphoribose; PSA:polar surface area; ADPR:adenosine 5'-diphosphoribose; AMP:adenosine monophosphate; ADP:adenosine diphosphate; ATP:adenosine triphosphate; SMILES:simplified molecular input line entry specification; SAR:structure–activity relationship; ANP:phosphoaminophosphonic acid-adenylate ester; TTP:thymidine-5'-triphosphate; DCP:2'-deoxycytidine-5'-triphosphate; DGT:2'-deoxyguanosine-5'-triphosphate; DTP:2'-deoxyadenosine 5'-triphosphate; DUP:synthesis of 2'-deoxyuridine 5'-(α,β -imido) triphosphate; ACP:phosphomethylphosphonic acid-adenylate ester; AD9:adenosine metavanadate; NAD:nicotinamide adenine dinucleotide; AGS:phosphothiothiophosphoric acid-adenylate ester; APC:phosphothiothiophosphoric acid-adenylate ester; AOV:adenosine diphosphate orthovanadate; USP:uridine-5'-monophosphate; UDP:uridine-5'-phosphate; UT-P:uridine-5'-triphosphate; 5GP:guanosine-5'-monophosphate; GDP:guanosine-5'-diphosphate; GTP:guanosine-5'-triphosphate; CSP:cytidine-5'-monophosphate; CDP:cytidine-5'-diphosphate; CTP:cytidine-5'-triphosphate; S6K1:S6 kinases RPS6KB1; PDE4B:phosphodiesterase 4B; PI3K α :phosphoinositide 3-kinase α ; CDK2:cyclin-dependent kinase 2

REFERENCES

- (1) Ward, R. A.; Fawell, S.; Floc'h, N.; Flemington, V.; McKerrecher, D.; Smith, P. D. Challenges and opportunities in cancer drug resistance. *Chem. Rev.* **2021**, *121*, 3297–3351.
- (2) Rafehi, M.; Neumann, A.; Baqi, Y.; Malik, E. M.; Wiese, M.; Namasivayam, V.; Müller, C. E. Molecular recognition of agonists and antagonists by the nucleotide-activated G protein-coupled P2Y2 receptor. *J. Med. Chem.* **2017**, *60*, 8425–8440.
- (3) Gregori-Puigjané, E.; Setola, V.; Hert, J.; Crews, B. A.; Irwin, J. J.; Lounkine, E.; Marnett, L.; Roth, B. L.; Shoichet, B. K. Identifying

mechanism-of-action targets for drugs and probes. *Proc. Natl. Acad. Sci. U.S.A.* **2012**, *109*, 11178–11183.

(4) Mendez, D.; Gaulton, A.; Bento, A. P.; Chambers, J.; De Veij, M.; Félix, E.; Magariños, M. P.; Mosquera, J. F.; Mutowo, P.; Nowotka, M.; Gordillo-Marañón, M.; Hunter, F.; Junco, L.; Mugumbate, G.; Rodriguez-Lopez, M.; Atkinson, F.; Bosc, N.; Radoux, Chris J.; Segura-Cabrera, A.; Hersey, A.; Leach, Andrew R. ChEMBL: towards direct deposition of bioassay data. *Nucleic Acids Res.* **2019**, *47*, D930–D940.

(5) Ujváry, I.; Hayward, J. BIOSTER: A database of bioisosteres and bioanalogues. *Bioisosteres Med. Chem.* **2012**, 53–74.

(6) Wirth, M.; Zoete, V.; Michielin, O.; Sauer, W. H. SwissBioisostere: a database of molecular replacements for ligand design. *Nucleic Acids Res.* **2013**, *41*, D1137–D1143.

(7) Tuyishime, M.; Lawrence, R.; Cocklin, S. Core chemotype diversification in the HIV-1 entry inhibitor class using field-based bioisosteric replacement. *Bioorg. Med. Chem. Lett.* **2016**, *26*, 228–234.

(8) Ertl, P. Identification of bioisosteric substituents by a deep neural network. *J. Chem. Inf. Model.* **2020**, *60*, 3369–3375.

(9) Groom, C. R.; Bruno, I. J.; Lightfoot, M. P.; Ward, S. C. The Cambridge Structural Database. *Acta Crystallogr., Sect. B: Struct. Sci., Cryst. Eng. Mater.* **2016**, *72*, 171–179.

(10) Cole, J. C.; Korb, O.; McCabe, P.; Read, M. G.; Taylor, R. Knowledge-based conformer generation using the Cambridge Structural Database. *J. Chem. Inf. Model.* **2018**, *58*, 615–629.

(11) Berman, H. M.; Westbrook, J.; Feng, Z.; Gilliland, G.; Bhat, T. N.; Weissing & Shindyalov Bourne, P. E. The Protein data bank. *Nucleic Acids Res.* **2000**, *28*, 235–242.

(12) Hunter, F. M. I.; Bento, A. P.; Bosc, N.; Gaulton, A.; Hersey, A.; Leach, A. R. Drug safety data curation and modeling in ChEMBL: Boxed warnings and withdrawn drugs. *Chem. Res. Toxicol.* **2021**, *34*, 385–395.

(13) Allen, F. H.; Groom, C. R.; Liebeschuetz, J. W.; Bardwell, D. A.; Olsson, T. S.; Wood, P. A. The hydrogen bond environments of 1H-tetrazole and tetrazolate rings: the structural basis for tetrazole-carboxylic acid bioisosterism. *J. Chem. Inf. Model.* **2012**, *52*, 857–866.

(14) Kennewell, E. A.; Willett, P.; Ducrot, P.; Luttmann, C. Identification of target-specific bioisosteric fragments from ligand-protein crystallographic data. *J. Comput.-Aided Mol. Des.* **2006**, *20*, 385–394.

(15) Seddon, M. P.; Cosgrove, D. A.; Gillet, V. J. Bioisosteric replacements extracted from high-quality structures in the protein databank. *ChemMedChem* **2018**, *13*, 607–613.

(16) Wood, D. J.; de Vlieg, J.; Wagener, M.; Ritschel, T. Pharmacophore fingerprint-based approach to binding site subpocket similarity and its application to bioisostere replacement. *J. Chem. Inf. Model.* **2012**, *52*, 2031–2043.

(17) Khashan, R. FragVLib a free database mining software for generating "Fragment-based Virtual Library" using pocket similarity search of ligand-receptor complexes. *J. Cheminform.* **2012**, *4*, 18.

(18) Desaphy, J.; Rognan, D. sc-PDB-Frag: a database of protein-ligand interaction patterns for Bioisosteric replacements. *J. Chem. Inf. Model.* **2014**, *54*, 1908–1918.

(19) Lešnik, S.; Škrlić, B.; Eržen, N.; Bren, U.; Gobec, S.; Konc, J.; Janežič, D. BoBER: web interface to the base of bioisosterically exchangeable replacements. *J. Cheminform.* **2017**, *9*, 62.

(20) Konc, J.; Janežič, D. ProBiS-ligands: a web server for prediction of ligands by examination of protein binding sites. *Nucleic Acids Res.* **2014**, *42*, W215–W220.

(21) Shan, J.; Pan, X.; Wang, X.; Xiao, X.; Ji, C. FragRep: A web server for structure-based drug design by fragment replacement. *J. Chem. Inf. Model.* **2020**, *60*, S900–S906.

(22) Del-Corso, A.; Cappiello, M.; Moschini, R.; Balestri, F.; Mura, U.; Ipata, P. L. The furanosidic scaffold of d-ribose: a milestone for cell life. *Biochem. Soc. Trans.* **2019**, *47*, 1931–1940.

(23) Abbas, C. A.; Sibirny, A. A. Genetic control of biosynthesis and transport of riboflavin and flavin nucleotides and construction of robust biotechnological producers. *Microbiol. Mol. Biol. Rev.* **2011**, *75*, 321–360.

(24) Xu, J.; Green, N. J.; Gibard, C.; Krishnamurthy, R.; Sutherland, J. D. Prebiotic phosphorylation of 2-thiouridine provides either nucleotides or DNA building blocks via photoreduction. *Nat. Chem.* **2019**, *11*, 457–462.

(25) Gustafsson, A. J.; Muraro, L.; Dahlberg, C.; Migaud, M.; Chevallier, O.; Khanh, H. N.; Krishnan, K.; Li, N.; Islam, M. S. ADP ribose is an endogenous ligand for the purinergic P2Y1 receptor. *Mol. Cell. Endocrinol.* **2011**, *333*, 8–19.

(26) Huang, C.; Hu, J.; Subedi, K. P.; Lin, A. H.; Paudel, O.; Ran, P.; Sham, J. S. Extracellular adenosine diphosphate ribose mobilizes intracellular Ca²⁺ via purinergic-dependent Ca²⁺ pathways in rat pulmonary artery smooth muscle cells. *Cell Physiol. Biochem.* **2015**, *37*, 2043–2059.

(27) Lee, H. C. Cyclic ADP-ribose and NAADP: fraternal twin messengers for calcium signaling. *Sci. China Life Sci.* **2011**, *54*, 699–711.

(28) Sun, Y.; Ke, Y.; Li, C.; Wang, J.; Tu, L.; Hu, L.; Jin, Y.; Chen, H.; Gong, J.; Yu, Z. Bifunctional and unusual amino Acid β - or γ -ester prodrugs of nucleoside analogues for improved affinity to ATB⁰⁺ and enhanced metabolic stability: An application to floxuridine. *J. Med. Chem.* **2020**, *63*, 10816–10828.

(29) Liao, A. M.; Cai, B.; Huang, J. H.; Hui, M.; Lee, K. K.; Lee, K. Y.; Chun, C. Synthesis, anticancer activity and potential application of diosgenin modified cancer chemotherapeutic agent cytarabine. *Food Chem. Toxicol.* **2021**, *148*, No. 111920.

(30) Holzer, S.; Rzechorzek, N. J.; Short, I. R.; Jenkyn-Bedford, M.; Pellegrini, L.; Kilkenny, M. L. Structural basis for inhibition of human primase by arabinofuranosyl nucleoside analogues fludarabine and vidarabine. *ACS Chem. Biol.* **2019**, *14*, 1904–1912.

(31) Hu, Y.; Liu, Y.; Coates, A. Azidothymidine produces synergistic activity in combination with colistin against antibiotic-resistant enterobacteriaceae. *Antimicrob. Agents Chemother.* **2019**, *63*, No. e01630-18.

(32) Miller, S. R.; Hau, R. K.; Jilek, J. L.; Morales, M. N.; Wright, S. H.; Cherrington, N. J. Nucleoside reverse transcriptase inhibitor interaction with human equilibrative nucleoside transporters 1 and 2. *Drug Metab. Dispos.* **2020**, *48*, 603–612.

(33) Young, C. K. J.; Wheeler, J. H.; Rahman, M. M.; Young, M. J. The antiretroviral 2',3'-dideoxycytidine causes mitochondrial dysfunction in proliferating and differentiated HepaRG human cell cultures. *J. Biol. Chem.* **2021**, *296*, No. 100206.

(34) Kandal, S.; Pannecouque, C.; Chapman, F. M.; Westwell, A. D.; McGuigan, C. Polyfluoroaromatic stavudine (d4T) ProTides exhibit enhanced anti-HIV activity. *Bioorg. Med. Chem. Lett.* **2019**, *29*, No. 126721.

(35) Somu, R. V.; Wilson, D. J.; Bennett, E. M.; Boshoff, H. I.; Celia, L.; Beck, B. J.; Barry, C. E., 3rd; Aldrich, C. C. Antitubercular nucleosides that inhibit siderophore biosynthesis: SAR of the glycosyl domain. *J. Med. Chem.* **2006**, *49*, 7623–7635.

(36) Zhang, B.; Wagner, G. K.; Weber, K.; Garnham, C.; Morgan, A. J.; Galione, A.; Guse, A. H.; Potter, B. V. 2'-deoxy cyclic adenosine 5'-diphosphate ribose derivatives: importance of the 2'-hydroxyl motif for the antagonistic activity of 8-substituted cADPR derivatives. *J. Med. Chem.* **2008**, *51*, 1623–1636.

(37) Guse, A. H. Second messenger function and the structure-activity relationship of cyclic adenosine diphosphoribose (cADPR). *FEBS J.* **2005**, *272*, 4590–4597.

(38) Bailey, V. C.; Fortt, S. M.; Summerhill, R. J.; Galione, A.; Potter, B. V. Cyclic aristeromycin diphosphate ribose: a potent and poorly hydrolysable Ca²⁺-mobilising mimic of cyclic adenosine diphosphate ribose. *FEBS Lett.* **1996**, *379*, 227–230.

(39) Currie, K. P.; Swann, K.; Galione, A.; Scott, R. H. Activation of Ca²⁺-dependent currents in cultured rat dorsal root ganglion neurones by a sperm factor and cyclic ADP-ribose. *Mol. Biol. Cell* **1992**, *3*, 1415–1425.

(40) Swarbrick, J. M.; Graeff, R.; Zhang, H.; Thomas, M. P.; Hao, Q.; Potter, B. V. Cyclic adenosine 5'-diphosphate ribose analogs without a "southern" ribose inhibit ADP-ribosyl cyclase-hydrolase CD38. *J. Med. Chem.* **2014**, *57*, 8517–8529.

- (41) Xu, J.; Yang, Z.; Dammermann, W.; Zhang, L.; Guse, A. H.; Zhang, L. H. Synthesis and agonist activity of cyclic ADP-ribose analogues with substitution of the northern ribose by ether or alkane chains. *J. Med. Chem.* **2006**, *49*, 5501–5512.
- (42) Guse, A. H. Cyclic ADP-ribose (cADPR) and nicotinic acid adenine dinucleotide phosphate (NAADP): novel regulators of Ca²⁺-signaling and cell function. *Curr. Mol. Med.* **2002**, *2*, 273–282.
- (43) Cakir-Kiefer, C.; Muller-Steffner, H.; Oppenheimer, N.; Schuber, F. Kinetic competence of the cADP-ribose-CD38 complex as an intermediate in the CD38/NAD⁺ glycohydrolase-catalysed reactions: implication for CD38 signalling. *Biochem. J.* **2001**, *358*, 399–406.
- (44) Tsuzuki, T.; Sakaguchi, N.; Kudoh, T.; Takano, S.; Uehara, M.; Murayama, T.; Sakurai, T.; Hashii, M.; Higashida, H.; Weber, K.; Guse, A. H.; Kameda, T.; Hirokawa, T.; Kumaki, Y.; Potter, B. V.; Fukuda, H.; Arisawa, M.; Shuto, S. Design and synthesis of cyclic ADP-4-thioribose as a stable equivalent of cyclic ADP-ribose, a calcium ion-mobilizing second messenger. *Angew. Chem., Int. Ed.* **2013**, *52*, 6633–6637.
- (45) Tromp, R. A.; van Ameijde, S.; Pütz, C.; Sundermann, C.; Sundermann, B.; von Frijtag Drabbe Künzel, J. K.; AP, I. J. Inhibition of nucleoside transport by new analogues of 4-nitrobenzylthioinosine: replacement of the ribose moiety by substituted benzyl groups. *J. Med. Chem.* **2004**, *47*, 5441–5450.
- (46) Dang, Q.; Kasibhatla, S. R.; Reddy, K. R.; Jiang, T.; Reddy, M. R.; Potter, S. C.; Fujitaki, J. M.; van Poelje, P. D.; Huang, J.; Lipscomb, W. N.; Erion, M. D. Discovery of potent and specific fructose-1,6-bisphosphatase inhibitors and a series of orally-bioavailable phosphoramidase-sensitive prodrugs for the treatment of type 2 diabetes. *J. Am. Chem. Soc.* **2007**, *129*, 15491–15502.
- (47) Reddy, M. R.; Erion, M. D. Relative binding affinities of fructose-1,6-bisphosphatase inhibitors calculated using a quantum mechanics-based free energy perturbation method. *J. Am. Chem. Soc.* **2007**, *129*, 9296–9297.
- (48) Erion, M. D.; Dang, Q.; Reddy, M. R.; Kasibhatla, S. R.; Huang, J.; Lipscomb, W. N.; van Poelje, P. D. Structure-guided design of AMP mimics that inhibit fructose-1,6-bisphosphatase with high affinity and specificity. *J. Am. Chem. Soc.* **2007**, *129*, 15480–15490.
- (49) Moreau, C.; Kirchberger, T.; Swarbrick, J. M.; Bartlett, S. J.; Fliegert, R.; Yorgan, T.; Bauche, A.; Harneit, A.; Guse, A. H.; Potter, B. V. Structure-activity relationship of adenosine 5'-diphosphoribose at the transient receptor potential melastatin 2 (TRPM2) channel: rational design of antagonists. *J. Med. Chem.* **2013**, *56*, 10079–10102.
- (50) Du, B.; Chan, C. M.; Lee, P. Y.; Cheung, L. H.; Xu, X.; Lin, Z.; Yu, W. Y. 2,2-difluorovinyl benzoates for diverse synthesis of gem-difluoroenol ethers by Ni-catalyzed cross-coupling reactions. *Nat. Commun.* **2021**, *12*, No. 412.
- (51) Malik, M. S.; Ahmed, S. A.; Althagafi, I. I.; Ansari, M. A.; Kamal, A. Application of triazoles as bioisosteres and linkers in the development of microtubule targeting agents. *RSC Med. Chem.* **2020**, *11*, 327–348.
- (52) Ertl, P. Craig plot 2.0: an interactive navigation in the substituent bioisosteric space. *J. Cheminform.* **2020**, *12*, 8.
- (53) Zhang, Y.; Borrel, A.; Ghemto, L.; Regad, L.; Boije Af Gennäs, G.; Camproux, A. C.; Yli-Kauhaluoma, J.; Xhaard, H. Structural isosteres of phosphate groups in the Protein data bank. *J. Chem. Inf. Model.* **2017**, *57*, 499–516.
- (54) Shan, J.; Ji, C. MolOpt: A web server for drug design using bioisosteric transformation. *Curr. Comput.-Aided Drug Des.* **2020**, *16*, 460–466.
- (55) Borrel, A.; Camproux, A. C.; Xhaard, H. Characterization of ionizable groups' environments in proteins and protein-ligand complexes through a statistical analysis of the Protein data bank. *ACS Omega* **2017**, *2*, 7359–7374.
- (56) Xu, Y.; Wang, S.; Hu, Q.; Gao, S.; Ma, X.; Zhang, W.; Shen, Y.; Chen, F.; Lai, L.; Pei, J. CavityPlus: a web server for protein cavity detection with pharmacophore modelling, allosteric site identification and covalent ligand binding ability prediction. *Nucleic Acids Res.* **2018**, *46*, W374–W379.
- (57) Johansson, N. G.; Turku, A.; Vidilaseris, K.; Dreano, L.; Khattab, A.; Ayuso Pérez, D.; Wilkinson, A.; Zhang, Y.; Tamminen, M.; Grazhdankin, E.; Kiriazis, A.; Fishwick, C. W. G.; Meri, S.; Yli-Kauhaluoma, J.; Goldman, A.; Boije Af Gennäs, G.; Xhaard, H. Discovery of membrane-bound pyrophosphatase inhibitors derived from an isoxazole fragment. *ACS Med. Chem. Lett.* **2020**, *11*, 605–610.
- (58) L & DeLano, W. PyMOL, 2.4; Schrödinger2020.
- (59) Laskowski, R. A.; Swindells, M. B. LigPlot+: multiple ligand-protein interaction diagrams for drug discovery. *J. Chem. Inf. Model.* **2011**, *51*, 2778–2786.
- (60) De Monte, C.; Carradori, S.; Bizzarri, B.; Bolasco, A.; Caprara, F.; Mollica, A.; Rivanera, D.; Mari, E.; Zicari, A.; Akdemir, A.; Secci, D. Anti-Candida activity and cytotoxicity of a large library of new N-substituted-1,3-thiazolidin-4-one derivatives. *Eur. J. Med. Chem.* **2016**, *107*, 82–96.
- (61) Couty, S.; Westwood, I. M.; Kalusa, A.; Cano, C.; Travers, J.; Boxall, K.; Chow, C. L.; Burns, S.; Schmitt, J.; Pickard, L.; Barillari, C.; McAndrew, P. C.; Clarke, P. A.; Linardopoulos, S.; Griffin, R. J.; Aherne, G. W.; Raynaud, F. I.; Workman, P.; Jones, K.; van Montfort, R. L. The discovery of potent ribosomal S6 kinase inhibitors by high-throughput screening and structure-guided drug design. *Oncotarget* **2013**, *4*, 1647–1661.
- (62) Bamford, M. J.; Alberti, M. J.; Bailey, N.; Davies, S.; Dean, D. K.; Gaiba, A.; Garland, S.; Harling, J. D.; Jung, D. K.; Panchal, T. A.; Parr, C. A.; Steadman, J. G.; Takle, A. K.; Townsend, J. T.; Wilson, D. M.; Witherington, J. (1H-imidazo[4,5-c]pyridin-2-yl)-1,2,5-oxadiazol-3-ylamine derivatives: a novel class of potent MSK-1-inhibitors. *Bioorg. Med. Chem. Lett.* **2005**, *15*, 3402–3406.
- (63) Bandarage, U.; Hare, B.; Parsons, J.; Pham, L.; Marhefka, C.; Bemis, G.; Tang, Q.; Moody, C. S.; Rodems, S.; Shah, S.; Adams, C.; Bravo, J.; Charonnet, E.; Savic, V.; Come, J. H.; Green, J. 4-(Benzimidazol-2-yl)-1,2,5-oxadiazol-3-ylamine derivatives: potent and selective p70S6 kinase inhibitors. *Bioorg. Med. Chem. Lett.* **2009**, *19*, 5191–5194.
- (64) Apsel, B.; Blair, J. A.; Gonzalez, B.; Nazif, T. M.; Feldman, M. E.; Aizenstein, B.; Hoffman, R.; Williams, R. L.; Shokat, K. M.; Knight, Z. A. Targeted polypharmacology: discovery of dual inhibitors of tyrosine and phosphoinositide kinases. *Nat. Chem. Biol.* **2008**, *4*, 691–699.
- (65) Cheng, H.; Li, C.; Bailey, S.; Baxi, S. M.; Goulet, L.; Guo, L.; Hoffman, J.; Jiang, Y.; Johnson, T. O.; Johnson, T. W.; Knighton, D. R.; Li, J.; Liu, K. K.; Liu, Z.; Marx, M. A.; Walls, M.; Wells, P. A.; Yin, M. J.; Zhu, J.; Zientek, M. Discovery of the highly potent PI3K/mTOR dual inhibitor PF-04979064 through structure-based drug design. *ACS Med. Chem. Lett.* **2013**, *4*, 91–97.
- (66) Arris, C. E.; Boyle, F. T.; Calvert, A. H.; Curtin, N. J.; Endicott, J. A.; Garman, E. F.; Gibson, A. E.; Golding, B. T.; Grant, S.; Griffin, R. J.; Jewsbury, P.; Johnson, L. N.; Lawrie, A. M.; Newell, D. R.; Noble, M. E.; Sausville, E. A.; Schultz, R.; Yu, W. Identification of novel purine and pyrimidine cyclin-dependent kinase inhibitors with distinct molecular interactions and tumor cell growth inhibition profiles. *J. Med. Chem.* **2000**, *43*, 2797–2804.
- (67) Pflug, A.; Gaudon, S.; Resa-Infante, P.; Lethier, M.; Reich, S.; Schulze, W. M.; Cusack, S. Capped RNA primer binding to influenza polymerase and implications for the mechanism of cap-binding inhibitors. *Nucleic Acids Res.* **2018**, *46*, 956–971.
- (68) Dalgarno, D.; Stehle, T.; Narula, S.; Schelling, P.; van Schravendijk, M. R.; Adams, S.; Andrade, L.; Keats, J.; Ram, M.; Jin, L.; Grossman, T.; MacNeil, I.; Metcalf, C., 3rd; Shakespeare, W.; Wang, Y.; Keenan, T.; Sundaramoorthi, R.; Bohacek, R.; Weigele, M.; Sawyer, T. Structural basis of Src tyrosine kinase inhibition with a new class of potent and selective trisubstituted purine-based compounds. *Chem. Biol. Drug Des.* **2006**, *67*, 46–57.
- (69) Song, M. S.; Kumar, G.; Shadrack, W. R.; Zhou, W.; Jeevan, T.; Li, Z.; Slavish, P. J.; Fabrizio, T. P.; Yoon, S. W.; Webb, T. R.; Webby, R. J.; White, S. W. Identification and characterization of influenza variants resistant to a viral endonuclease inhibitor. *Proc. Natl. Acad. Sci. U.S.A.* **2016**, *113*, 3669–3674.
- (70) Omoto, S.; Speranzini, V.; Hashimoto, T.; Noshi, T.; Yamaguchi, H.; Kawai, M.; Kawaguchi, K.; Uehara, T.; Shishido, T.; Naito, A.; Cusack, S. Characterization of influenza virus variants induced by

treatment with the endonuclease inhibitor baloxavir marboxil. *Sci. Rep.* **2018**, *8*, No. 9633.

(71) Jones, J. C.; Kumar, G.; Barman, S.; Najera, I.; White, S. W.; Webby, R. J.; Govorkova, E. A. Identification of the I38T PA substitution as a resistance marker for next-generation influenza virus endonuclease inhibitors. *mBio* **2018**, *9*, No. e00430-18.

(72) Wang, H.; Luo, X.; Ye, M.; Hou, J.; Robinson, H.; Ke, H. Insight into binding of phosphodiesterase-9A selective inhibitors by crystal structures and mutagenesis. *J. Med. Chem.* **2010**, *53*, 1726–1731.

(73) Liu, S.; Mansour, M. N.; Dillman, K. S.; Perez, J. R.; Danley, D. E.; Aeed, P. A.; Simons, S. P.; Lemotte, P. K.; Menniti, F. S. Structural basis for the catalytic mechanism of human phosphodiesterase 9. *Proc. Natl. Acad. Sci. U.S.A.* **2008**, *105*, 13309–13314.

(74) Kumar, A.; Mandiyan, V.; Suzuki, Y.; Zhang, C.; Rice, J.; Tsai, J.; Artis, D. R.; Ibrahim, P.; Bremer, R. Crystal structures of proto-oncogene kinase Pim1: a target of aberrant somatic hypermutations in diffuse large cell lymphoma. *J. Mol. Biol.* **2005**, *348*, 183–193.

(75) Parker, L. J.; Taruya, S.; Tsuganezawa, K.; Ogawa, N.; Mikuni, J.; Honda, K.; Tomabechi, Y.; Handa, N.; Shirouzu, M.; Yokoyama, S.; Tanaka, A. Kinase crystal identification and ATP-competitive inhibitor screening using the fluorescent ligand SKF86002. *Acta Crystallogr., Sect. D: Biol. Crystallogr.* **2014**, *70*, 392–404.

(76) Holder, S.; Zemskova, M.; Zhang, C.; Tabrizizad, M.; Bremer, R.; Neidigh, J. W.; Lilly, M. B. Characterization of a potent and selective small-molecule inhibitor of the PIM1 kinase. *Mol. Cancer Ther.* **2007**, *6*, 163–172.

(77) Card, G. L.; England, B. P.; Suzuki, Y.; Fong, D.; Powell, B.; Lee, B.; Luu, C.; Tabrizizad, M.; Gillette, S.; Ibrahim, P. N.; Artis, D. R.; Bollag, G.; Milburn, M. V.; Kim, S. H.; Schlessinger, J.; Zhang, K. Y. Structural basis for the activity of drugs that inhibit phosphodiesterases. *Structure* **2004**, *12*, 2233–2247.

(78) Good, A. C.; Liu, J.; Hirth, B.; Asmussen, G.; Xiang, Y.; Biemann, H. P.; Bishop, K. A.; Fremgen, T.; Fitzgerald, M.; Gladysheva, T.; Jain, A.; Jancsics, K.; Metz, M.; Papoulis, A.; Skerlj, R.; Stepp, J. D.; Wei, R. R. Implications of promiscuous Pim-1 kinase fragment inhibitor hydrophobic interactions for fragment-based drug design. *J. Med. Chem.* **2012**, *55*, 2641–2648.

(79) Wang, X.; Magnuson, S.; Pastor, R.; Fan, E.; Hu, H.; Tsui, V.; Deng, W.; Murray, J.; Steffek, M.; Wallweber, H.; Moffat, J.; Drummond, J.; Chan, G.; Harstad, E.; Ebens, A. J. Discovery of novel pyrazolo[1,5-a]pyrimidines as potent pan-Pim inhibitors by structure- and property-based drug design. *Bioorg. Med. Chem. Lett.* **2013**, *23*, 3149–3153.

(80) Knight, S. D.; Adams, N. D.; Burgess, J. L.; Chaudhari, A. M.; Darcy, M. G.; Donatelli, C. A.; Luengo, J. I.; Newlander, K. A.; Parrish, C. A.; Ridgers, L. H.; Sarpong, M. A.; Schmidt, S. J.; Van Aller, G. S.; Carson, J. D.; Diamond, M. A.; Elkins, P. A.; Gardiner, C. M.; Garver, E.; Gilbert, S. A.; Gontarek, R. R.; Jackson, J. R.; Kershner, K. L.; Luo, L.; Raha, K.; Sherk, C. S.; Sung, C. M.; Sutton, D.; Tummino, P. J.; Wegrzyn, R. J.; Auger, K. R.; Dhanak, D. Discovery of GSK2126458, a highly potent inhibitor of PI3K and the mammalian target of rapamycin. *ACS Med. Chem. Lett.* **2010**, *1*, 39–43.

(81) Pierce, A. C.; Jacobs, M.; Stuver-Moody, C. Docking study yields four novel inhibitors of the protooncogene Pim-1 kinase. *J. Med. Chem.* **2008**, *51*, 1972–1975.

(82) Huber, K.; Brault, L.; Fedorov, O.; Gasser, C.; Filippakopoulos, P.; Bullock, A. N.; Fabbro, D.; Trappe, J.; Schwaller, J.; Knapp, S.; Bracher, F. 7,8-dichloro-1-oxo- β -carbolines as a versatile scaffold for the development of potent and selective kinase inhibitors with unusual binding modes. *J. Med. Chem.* **2012**, *55*, 403–413.

(83) Lama, L.; Adura, C.; Xie, W.; Tomita, D.; Kamei, T.; Kuryavyi, V.; Gogakos, T.; Steinberg, J. I.; Miller, M.; Ramos-Espiritu, L.; Asano, Y.; Hashizume, S.; Aida, J.; Imaeda, T.; Okamoto, R.; Jennings, A. J.; Michino, M.; Kuroita, T.; Stamford, A.; Gao, P.; Meinke, P.; Glickman, J. F.; Patel, D. J.; Tuschl, T. Development of human cGAS-specific small-molecule inhibitors for repression of dsDNA-triggered interferon expression. *Nat. Commun.* **2019**, *10*, No. 2261.

(84) Alphey, M. S.; Pirrie, L.; Torrie, L. S.; Boulkeroua, W. A.; Gardiner, M.; Sarkar, A.; Maringer, M.; Oehlmann, W.; Brenk, R.;

Scherman, M. S.; McNeil, M.; Rejzek, M.; Field, R. A.; Singh, M.; Gray, D.; Westwood, N. J.; Naismith, J. H. Allosteric competitive inhibitors of the glucose-1-phosphate thymidyltransferase (RmlA) from *Pseudomonas aeruginosa*. *ACS Chem. Biol.* **2013**, *8*, 387–396.

(85) Wyatt, P. G.; Woodhead, A. J.; Berdini, V.; Boulstridge, J. A.; Carr, M. G.; Cross, D. M.; Davis, D. J.; Devine, L. A.; Early, T. R.; Feltell, R. E.; Lewis, E. J.; McMenamin, R. L.; Navarro, E. F.; O'Brien, M. A.; O'Reilly, M.; Reule, M.; Saxty, G.; Seavers, L. C.; Smith, D. M.; Squires, M. S.; Trewartha, G.; Walker, M. T.; Woolford, A. J. Identification of N-(4-piperidinyl)-4-(2,6-dichlorobenzoylamino)-1H-pyrazole-3-carboxamide (AT7519), a novel cyclin dependent kinase inhibitor using fragment-based X-ray crystallography and structure based drug design. *J. Med. Chem.* **2008**, *51*, 4986–4999.

(86) Engh, R. A.; Girod, A.; Kinzel, V.; Huber, R.; Bossemeyer, D. Crystal structures of catalytic subunit of cAMP-dependent protein kinase in complex with isoquinolinesulfonyl protein kinase inhibitors H7, H8, and H89. Structural implications for selectivity. *J. Biol. Chem.* **1996**, *271*, 26157–26164.

(87) Elias, T. C.; de Oliveira, H. C. B.; da Silveira, N. J. F. MB-Isoster: A software for bioisosterism simulation. *J. Comput. Chem.* **2018**, *39*, 2481–2487.